https://doi.org/10.5194/egusphere-2024-4093
Preprint. Discussion started: 22 January 2025

Representation of a two-way coupled irrigation system in the Common Land Model

Shulei Zhang[1,*,#], Hongbin Liang[1,*,#], Fang Li[2], Xingjie Lu[1], Yongjiu Dai[1]

[1] *Southern Marine Science and Engineering Guangdong Laboratory (Zhuhai), School of Atmospheric Sciences, Sun Yat-sen University, Guangzhou, China*

[2]*International Center for Climate and Environment Sciences, Institute of Atmospheric Physics, Chinese Academy of Sciences, Beijing, 100029, China*

[*] ***Corresponding Authors:*** *Shulei Zhang (zhangshlei@mail.sysu.edu.cn) & Hongbin Liang (lianghb25@mail2.sysu.edu.cn)*

[#] *These authors contributed equally to this work.*

Abstract

Human land–water management, especially irrigation water withdrawal and use, significantly impacts the global and regional water cycle, energy budget, and near-surface climate. While land surface models are widely used to explore and predict the impacts of irrigation, the irrigation system representation in these models is still in its early stages. This study enhances the Common Land Model (CoLM) by introducing a two-way coupled irrigation module. This module includes an irrigation water demand scheme based on soil moisture deficit, an irrigation application scheme considering four major irrigation methods, and an irrigation water withdrawal scheme that incorporates multiple water source constraints by integrating CoLM with a river routing model and a reservoir operation scheme. Crucially, it explicitly accounts for the feedback between irrigation water demand and supply, which is constrained by available surface water (i.e., runoff, streamflow, reservoir storage) and groundwater. Simulations conducted from 2001 to 2016 at a 0.25° spatial resolution across the contiguous United States reveal that the model effectively reproduces irrigation withdrawals, their spatial distribution, and water source proportions, aligning well with reported state-level statistics. Comprehensive validation demonstrates that the new module significantly improves model accuracy in simulating regional energy dynamics (sensible heat, latent heat, and surface temperature), hydrology (river flow), and agricultural outputs (yields for maize, soybean, and wheat). Application analyses highlight the potential of the enhanced CoLM as a valuable tool for predicting irrigation-driven climate impacts and assessing water use and scarcity. This research offers a pathway for a more holistic representation of fluxes in irrigated areas and human-water interactions within land surface models. It is valuable for exploring the interconnected evolution of climate, water resources, agricultural production, and irrigation activities, while supporting sustainable water management decisions in a changing climate.

https://doi.org/10.5194/egusphere-2024-4093
Preprint. Discussion started: 22 January 2025

1. Introduction

Freshwater resources are indispensable for human society. Since 1900, the global population has increased more than fourfold, leading to a nearly sixfold rise in water withdrawals, from approximately 500 km³ per year in 1900 to about 3000 km³ per year in 2000, with agriculture being the dominant water user (Pokhrel et al., 2016). Around 70% of global freshwater has been withdrawn for irrigation (Campbell et al., 2017), accounting for 90% of consumptive water use (Siebert and Döll, 2010), with irrigated areas providing approximately 40% of global food production on just 2.5% of global land (Abdullah, 2006). Accompanied by significant socioeconomic benefits, these intense human land-water management practices have profoundly altered Earth's surface and impacted terrestrial water and energy cycles (Ketchum et al., 2023; Nocco et al., 2019; Rappin et al., 2022; Thiery et al., 2017; de Vrese et al., 2016). The demand for irrigation water is anticipated to rise with the growing global population and food demand, while climate-warming-induced droughts are likely to exacerbate this need (McDermid et al., 2023; Mehta et al., 2024; Yang et al., 2023). Therefore, understanding and quantifying the impacts of irrigation water management in human-Earth system interactions are crucial for developing strategies to sustainably manage these resources amidst changing climatic and demographic conditions.

Irrigation practices transfer water from various sources, such as rivers, lakes, reservoirs, and aquifers, into agricultural systems, directly affecting the magnitude and timing of runoff and river flow (Ketchum et al., 2023). The rising irrigation demand has spurred increased construction of reservoirs and diversions, resulting in both local and downstream impacts. In some regions, water extraction for irrigation has reduced the availability of both surface and groundwater (Döll et al., 2014). Besides modifying water fluxes, irrigation also influences regional climates both locally and remotely. Locally, it alters surface albedo, evapotranspiration, and surface soil moisture, impacting regional radiation and energy balances and affecting temperature, humidity, and precipitation through land-atmosphere feedback (Chen and Dirmeyer, 2019; Kang and Eltahir, 2018; Li et al., 2022; McDermid et al., 2017; Nocco et al., 2019). Remotely, it affects climate through complex interactions between altered temperature and moisture gradients and larger-scale processes such as atmospheric circulation and wave activity (Douglas et al., 2009; Phillips et al., 2022; de Vrese et al., 2016).

Earth system models (ESMs) are powerful tools for examining the interactions and feedback among the intricately intertwined processes of the Earth system, both in the past and future. Land surface models (LSMs) are a crucial component of ESMs. Due to the complex dynamics of natural hydrological processes and anthropogenic activities, describing human-water interactions has been recognized as a significant challenge in Land surface modeling (Nazemi and Wheater, 2015). In recent years, targeted efforts have aimed to address this deficiency, yet water use remains largely underrepresented or in a nascent stage within LSMs (Blyth et al., 2021; Taranu et al., 2024). Meanwhile, global hydrological models (GHMs), originally designed for water

https://doi.org/10.5194/egusphere-2024-4093
Preprint. Discussion started: 22 January 2025

resource assessment, have undergone continuous improvements over the last three decades to explicitly represent human water use (Hanasaki et al., 2018; Liang et al., 1994; Müller Schmied et al., 2021; Sood and Smakhtin, 2015; Sutanudjaja et al., 2018; Tang et al., 2007). These models enable the determination of the spatial distribution and temporal evolution of water resources and water stress for both humans and other biota under the pressures of global change (Döll et al., 2018; Schewe et al., 2014; Schlosser et al., 2014). These advancements have offered valuable insights for incorporating human water use into LSMs.

Parameterizing irrigation water use and modeling its impacts in GHMs and LSMs has been approached using different assumptions and simplifications in three key aspects: irrigation demands, irrigation methods, and irrigation water supplies/withdrawals. The first aspect is estimating irrigation water demands. Models estimate these demands using either a root-zone soil moisture deficit approach or a crop-specific potential evapotranspiration approach. The root-zone soil moisture deficit approach estimates irrigation demand as the water needed to keep root-zone soil moisture (usually within the top meter of soil) above a certain threshold during the growing season (normally a certain percentage of field capacity or soil saturation) (Ozdogan et al., 2010). The crop-specific potential evapotranspiration approach estimates irrigation needs based on the difference between crop-specific potential evapotranspiration and simulated unirrigated evapotranspiration, or between potential and effective precipitation under well-watered conditions where crops transpire at their maximum rate (Müller Schmied et al., 2021). Notably, LSMs generally do not use potential evapotranspiration to estimate irrigation demand.

The second aspect concerns the representation of irrigation methods. Many models simplify irrigation application by directly modifying soil moisture or treating it as additional rainfall across all irrigated land, overlooking the diversity of irrigation techniques employed in various parts of the world or by different farmers (Li et al., 2024; Lu et al., 2015; de Vrese et al., 2018). Recently, some models have started integrating specific irrigation techniques for certain crops or regions. For instance, LPJmL includes sprinkler, drip, and surface irrigation methods, and CLM incorporates drip, sprinkler, flood, and paddy irrigation methods (Jägermeyr et al., 2015; Yao et al., 2022). Different irrigation techniques affect farmland hydrological processes and irrigation efficiency in distinct ways. For example, drip and surface irrigation methods avoid interception losses observed with sprinkler (Nair et al., 2013).

Third is the representation of irrigation water supplies/withdrawals, which is particularly critical as it involves the interaction between multiple processes or modules, such as hydrological and agricultural systems. However, explicit representation of these interactions remains largely absent in LSMs, despite the extensive modeling experience provided by GHMs. Such modeling first requires identifying the sources of irrigation water, typically categorized into surface water and groundwater. Surface water sources are normally constrained by available runoff, streamflow, and storage such as lakes and reservoirs. Accessing these sources, such as rivers and reservoirs, necessitates coupling with river routing and reservoir modules, which are well-

https://doi.org/10.5194/egusphere-2024-4093
Preprint. Discussion started: 22 January 2025

represented in many GHMs (Biemans et al., 2011; Hanasaki et al., 2018). Groundwater is typically divided into renewable sources (baseflow or dynamic groundwater levels) and nonrenewable sources (fossil groundwater). Some models assume an inexhaustible supply of nonrenewable groundwater to meet irrigation demands, neglecting irrigation shortages caused by water scarcity (Zhou et al., 2020). Additionally, some GHMs incorporate alternative sources, such as inter-regional water transfers and seawater desalination (Hanasaki et al., 2018; Sutanudjaja et al., 2018). A second critical aspect of irrigation water supply modeling is determining the allocation of irrigation water among different sources, including the prioritization of water usage. Various models adopt different assumptions for this allocation. For example, H08 prioritizes surface water (Hanasaki et al., 2018), while WBMplus prioritizes reservoirs and groundwater (Wisser et al., 2010). PCR-GLOBWB uses an empirical approach that allocates groundwater use based on comparisons between baseflow conditions and long-term historical climatology, capturing feedback between water supply and demand (Sutanudjaja et al., 2018). Another common approach is to assume a predefined allocation ratio based on water withdrawal infrastructure (e.g., Siebert et al., 2010), using this ratio to divide total irrigation abstractions between groundwater and surface water (Arboleda-Obando et al., 2024; Leng et al., 2015). Despite these advances, the representation of water extraction and the coupling of irrigation and hydrological systems in LSMs is still in its early stages. Most irrigation-enabled models still assume an unlimited water supply, failing to account for constraints imposed by water availability (Druel et al., 2022; Yao et al., 2022; Zhou et al., 2020).

The Common Land Model (CoLM; Dai et al., 2003), derived from the Community Land Model (CLM), is a widely used land surface model that integrates ecological, hydrological, and biophysical processes. In recent years, it has further incorporated various physical processes such as lakes, wetlands, and dynamic vegetation, enhancing the representation of energy and water exchanges among soil, vegetation, snow, and atmosphere. CoLM has been successfully implemented in global atmospheric models, such as GRAPES, CWRF, and CAS-ESM2.0 (Shen et al., 2021; Yuan and Liang, 2011; Zhang et al., 2020a). Despite significant advancements in parameterizing natural land surface processes, the representation of human activities in CoLM remains at an early stage. Recently, CoLM has further integrated a crop module, providing a foundation for considering irrigation and its interactions with natural water systems.

To enhance the representation of human–water interactions in land surface models, we introduce a new irrigation module for CoLM. This module provides a comprehensive framework for simulating the entire irrigation water system, including water demand, withdrawal, and utilization. It incorporates an irrigation water demand scheme based on soil moisture deficits, an irrigation application scheme accounting for four major irrigation methods, and an irrigation water withdrawal scheme that incorporates multiple water source constraints by integrating CoLM with a river routing model and a reservoir operation scheme. A key focus of this module is the bidirectional coupling between irrigation water demand and supply, alongside a detailed representation of water withdrawals from different sources. Section 2 provides a detailed

https://doi.org/10.5194/egusphere-2024-4093
Preprint. Discussion started: 22 January 2025

description of the module and its implementation, including an overview of CoLM, the datasets used for simulation and validation, and the experimental design. Section 3 validates the module's performance in simulating irrigation water withdrawals using reported data and compares its results to other hydrological models. It also assesses improvements in model accuracy for regional energy dynamics (sensible heat, latent heat, and surface temperature), hydrology (river flow), and agricultural outputs (maize, soybean, and wheat yields). Section 4 demonstrates two key applications of the module: analyzing irrigation impacts on the energy budget and evaluating irrigation water security. Finally, we discuss the module's current limitations and propose potential future improvements.

2. Materials and Methods

2.1 Description of CoLM and its crop module

The Common Land Model (CoLM) is one of the most advanced land surface models widely used to simulate the Water–Energy–Carbon Nexus. The original version of CoLM (Dai et al., 2003) combines the three land surface models: the Land Surface Model (LSM; Bonan, 1996), the Biosphere-Atmosphere Transfer Scheme (BATS; Dickinson et al., 1993), and the 1994 version of the Chinese Academy of Sciences Institute of Atmospheric Physics LSM (IAP94; Dai and Zeng, 1997). CoLM2014 integrates the Catchment-Based Macro-Scale Floodplain model (CaMa-Flood; Yamazaki et al., 2011), enabling river routing calculations within the model. Specifically, runoff generated by CoLM is transferred to CaMa-Flood for routing through the river network. CaMa-Flood represents the river network as a series of irregular unit catchments, defined through sub-grid topographic parameters. River discharge and other flow characteristics are computed using the local inertial equations along the river network, allowing for detailed flow dynamics across catchments.

The CoLM2024 version incorporates substantial updates over CoLM2014, particularly by introducing representations of biogeochemical cycles and human activity processes (e.g., crop growth and reservoir management). The new crop module introduces a phenological development scheme based on accumulated temperature, a biomass allocation scheme among different plant organs, and fertilization schemes (Drewniak et al., 2013). Crops are categorized into four organ pools: leaves, stems, fine roots, and grains. The growth stages are divided into three phases: sowing to emergence, emergence to grain filling, and grain filling to maturity, with carbon allocation ratios to roots, stems, leaves, and grains varying across these phases. Upon maturation, crops are harvested, with part of the carbon from the grains contributing to the yield, while a small portion (3g) is reserved as seeds for the next growing season. For carbon assimilation, the module employs Farquhar's photosynthesis scheme (Collatz et al., 1992; Farquhar et al., 1980) and Ball-Berry's stomatal model (Ball et al., 1987; Collatz et al., 1991), treating maize as a C4 crop and other crops as C3. Additionally, the module accounts for the effects of heat stress, water stress, nitrogen stress, and ozone stress on yield (Li et al., 2024;

https://doi.org/10.5194/egusphere-2024-4093
Preprint. Discussion started: 22 January 2025

Lombardozzi et al., 2020). The module has been calibrated for various crops, including maize, soybean, spring and winter wheat, rice, cotton, and sugarcane, enabling accurate simulation of crop yields.

2.2 Two-way coupled irrigation water use module

2.2.1 Irrigation demand

The irrigation demand is calculated using the soil moisture deficit method (Leng et al., 2017; Ozdogan et al., 2010; Yao et al., 2022). During the crop growth stage, irrigation is triggered at 6 a.m. local time if the soil moisture in the root zone (z_{irrig}=1m) falls below the threshold value (ω_{thresh}). The total irrigation water demand (D_{irrig}, mm) is then calculated using Equation (1):

$$D_{irrig} = \begin{cases} \omega_{irrig} - \omega_{avail} & \omega_{avail} \leqslant \omega_{thresh} \\ 0 & \omega_{avail} > \omega_{thresh} \end{cases} \tag{1}$$

where ω_{avail} is the total soil water amount in the root zone (mm); ω_{irrig} is the irrigation target threshold (mm), calculated using Equation (2):

$$\omega_{irrig} = f_{irrig}(\omega_{target} - \omega_{wilt}) + \omega_{wilt} \tag{2}$$

where ω_{wilt} is the wilting point soil water amount in the root zone (mm), calculated as the sum of soil water at the wilting point for each soil layer ($\sum_{j=1}^{N_{irr}} \theta_{wilt}\Delta z_j$); ω_{target} is the target soil water amount in the root zone (mm), calculated as the sum of target soil water for each soil layer ($\sum_{j=1}^{N_{irr}} \theta_{target}\Delta z_j$). N_{irr} is the number of soil layers in the root zone and Δz_j is the thickness of each soil layer (m). The target (θ_{target}) and wilting point (θ_{wilt}) soil moisture (m^3/m^3) for each layer are calculated based on the corresponding soil water potential (Φ_{target} and Φ_{wilt}). f_{irrig} is a weighting coefficient ranging from 0 to 1, controlling the extent to which soil water amount approaches the target level ω_{target} during irrigation (default value = 1). In some cases, it can represent the efficiency of the irrigation system, accounting for water losses due to evaporation, seepage, or other factors.

The irrigation trigger threshold (ω_{thresh}) in Equation (1) is calculated as:

$$\omega_{thresh} = f_{thresh}(\omega_{trigger} - \omega_{wilt}) + \omega_{wilt} \tag{3}$$

where $\omega_{trigger}$ is the trigger water amount in the root zone (mm); f_{thresh} is also a weighting coefficient ranging from 0 to 1 that controls the proximity of soil water amount to the trigger level $\omega_{trigger}$ (default value = 1).

https://doi.org/10.5194/egusphere-2024-4093
Preprint. Discussion started: 22 January 2025

The values of ω_{trigger} and ω_{target} are set according to the irrigation application method. For drip and sprinkler irrigation, both ω_{trigger} and ω_{target} are set to the soil field capacity water amount. For flood irrigation, ω_{trigger} is set to the soil field capacity water amount and ω_{target} to the saturation water amount. For paddy irrigation, both ω_{trigger} and ω_{target} are set to the saturation water amount.

2.2.2 Irrigation application

The model incorporates four different irrigation application methods: drip irrigation, sprinkler irrigation, flood irrigation, and paddy irrigation, each with unique triggering conditions, water demand requirements, and application processes. Drip irrigation is triggered when soil moisture in the root zone falls below field capacity, with the irrigation goal being to restore soil moisture to field capacity. This method applies water directly to the surface soil, allowing it to percolate into deeper soil layers. Sprinkler irrigation shares the same triggering condition and demand requirement as drip irrigation but applies water above the canopy. In this method, water can be intercepted and evaporated before reaching the soil surface, resulting in relatively lower irrigation efficiency. This method is the most commonly used in the United States. Flood irrigation is triggered when soil moisture falls below field capacity, to raise soil moisture to the point of saturation. Paddy irrigation is applied whenever soil moisture drops below saturation, aiming to restore soil moisture to saturation without causing runoff loss. Paddy fields are typically maintained with a specific water level on the surface (10 cm) during the growing season. A global irrigation method map (Yao et al., 2022; Figure S3) is used to determine the irrigation method for each grid. In addition, irrigation is implemented daily at 6 a.m., if necessary, with water supply evenly distributed across each time step throughout the next 4 hours.

2.2.3 Irrigation water supply/withdrawal

The model incorporates two distinct irrigation water supply/withdrawal schemes. The first scheme, Unlimited Supply (irrig-unlim), assumes that irrigation demand is fully met without accounting for specific water sources, a common approach in most land surface models (Yao et al., 2022). The second scheme, Limited Supply (irrig-lim), divides total irrigation demand between surface water and groundwater sources, labeled as surface water demand (D_{surf}) and groundwater demand (D_{grnd}), respectively. Both demands are constrained by the available water within each respective system. This distribution is based on the spatial extent of groundwater irrigation equipment, as provided by Siebert et al. (2010), and is formulated as follows:

$$D_{\text{surf}} = D_{\text{irrig}} \times (1 - f_{\text{grnd}}) \tag{4}$$

$$D_{\text{grnd}} = D_{\text{irrig}} \times f_{\text{grnd}} \tag{5}$$

https://doi.org/10.5194/egusphere-2024-4093
Preprint. Discussion started: 22 January 2025

where D_{surf} and D_{grnd} represent the demand from surface water and groundwater systems, and f_{grnd} denotes the area fraction covered by groundwater equipment. In this scheme, surface water demand (D_{surf}) is sourced sequentially from local grid cell runoff, local river streamflow, and upstream reservoirs, while groundwater demand (D_{grnd}) is drawn from groundwater aquifers.

2.2.3.1 Surface water supply

In our two-way coupled irrigation system (Figure 1), the daily surface water supply for irrigation is constrained by surface water availability, which is simulated by CoLM (runoff) and CaMa-Flood (local streamflow and upstream reservoirs). We first examine whether the runoff from the local grid cell (S_{ro}) can meet the daily surface water demand (D_{surf}) for that cell. If runoff is insufficient, additional water is sourced from local streamflow and upstream reservoirs. River streamflow availability (S_{riv}) is determined by CaMa-Flood. For each irrigated grid cell, the river grid with the highest flow within a 250 km radius is selected as the source. To prevent excessive water extraction, a withdrawal limit is imposed, ensuring that the remaining flow in each river grid cell does not drop below 20% of its average daily volume. Before conducting irrigation simulations, natural river flow simulations are performed to establish essential parameters for both river and reservoir water withdrawal schemes.

Reservoir water availability (S_{res}) is also determined by CaMa-Flood, which now includes a reservoir module. This module consists of the following components: (i) a reservoir dataset that provides reservoir location information matched with the river network, along with reservoir parameters (e.g., characteristic storage capacity); (ii) a reservoir operation scheme designed for flood control; and (iii) a routing scheme that integrates reservoir operations into river flow simulations. For more details, refer to Hanazaki et al. (2022). In this study, we further propose a new scheme for sourcing irrigation water from reservoirs (Figure 2), which involves the following steps:

(i) Identifying the irrigation area served by each reservoir. It is challenging to accurately define the true irrigation extent/area for each reservoir, especially across large spatial domains. Therefore, a simplified approach is adopted here: larger reservoirs are assumed to cover a proportionately larger irrigation area, restricted to downstream regions only (since upstream water transfer is economically infeasible). Based on the relationship between reservoir size and the corresponding irrigation area provided in Table S1, we calculate the irrigation area for each reservoir according to its storage capacity by linear interpolation. Downstream irrigation grids are selected sequentially, from nearest to farthest, until the cumulative grid area closely matches the calculated irrigation area. If multiple reservoirs serve the same irrigation grid, a sharing proportion (f_{share}, ranging from 0 to 1) is assigned to the irrigation grid based on the degree of shared usage.

https://doi.org/10.5194/egusphere-2024-4093
Preprint. Discussion started: 22 January 2025

(ii) Calculating the irrigation demand for each reservoir by aggregating the demands of associated irrigation grids. This is expressed as: $D_{\text{res-total}} = \sum_{i=1}^{N}\left(D_{\text{irrig-unmet}}^{\text{i}} \times f_{\text{share}}^{\text{i}}\right)$, where $D_{\text{irrig-unmet}}^{\text{i}}$ and $f_{\text{share}}^{\text{i}}$ represent the irrigation demand (i.e., the portion of D_{surf} not met by local runoff and river streamflow) and sharing proportion of grid *i*, respectively. *N* denotes the number of irrigation grids served by the reservoir.

(iii) Executing reservoir withdrawals for irrigation based on demands. Water is then withdrawn ($S_{\text{res-total}}$) from the reservoir's effective storage (V_{eff}) — the portion between the current water level and dead water level—according to the required demand. This is expressed as $S_{\text{res-total}} = \min(D_{\text{res-total}}, V_{\text{eff}})$. After updating the reservoir storage, the reservoir operation and subsequent river routing are calculated following the approach outlined in Hanazaki et al. (2022).

(iv) Redistributing withdrawn water to the irrigation grids. Based on each irrigation grid's contribution to the total reservoir irrigation demand, the total withdrawal volume is proportionally allocated across the associated grids ($S_{\text{res}}^{\text{i}}$). This is expressed as $S_{\text{res}}^{\text{i}} = S_{\text{res-total}} \times \frac{D_{\text{irrig-unmet}}^{\text{i}} \times f_{\text{share}}^{\text{i}}}{D_{\text{res-total}}}$. Notably, this water is not applied directly to irrigation but is stored in a temporary reservoir (i.e., a temporary variable) for each irrigation grid in CoLM. This approach addresses the response delay in water supply from the river routing model to the land model's irrigation demands, as the time step for CoLM is 60 minutes, while CaMa-Flood operates with a 6-hour time step and exchanges information with CoLM every 6 hours. Moreover, if the reservoir cannot fully meet the irrigation demand within the initial time step, any unmet demand is carried forward to the next time step. This process continues over a 24-hour cycle, after which new water demands for the next day are received.

Thus, the computational sequence proceeds as follows: Step (i) is completed before model execution, with its results serving as an essential input for the irrigation module. During model operation, CoLM calculates the irrigation demand at 6 a.m. local time. The unmet demand (after subtracting the water supplied by local runoff and streamflow) is then sent to CaMa-Flood, as described in Step (ii). CaMa-Flood supplies water from reservoir to meet this demand, as described in Step (iii), and returns the supplied water to CoLM according to Step (iv), over the next 24 hours. During this process, the water supplied by reservoir is stored in the temporary reservoir (variable) for each irrigation grid within CoLM. The following day, when irrigation begins again at 6 a.m., water is withdrawn directly from the temporary reservoir if the demand cannot be met by local runoff and streamflow.

https://doi.org/10.5194/egusphere-2024-4093
Preprint. Discussion started: 22 January 2025

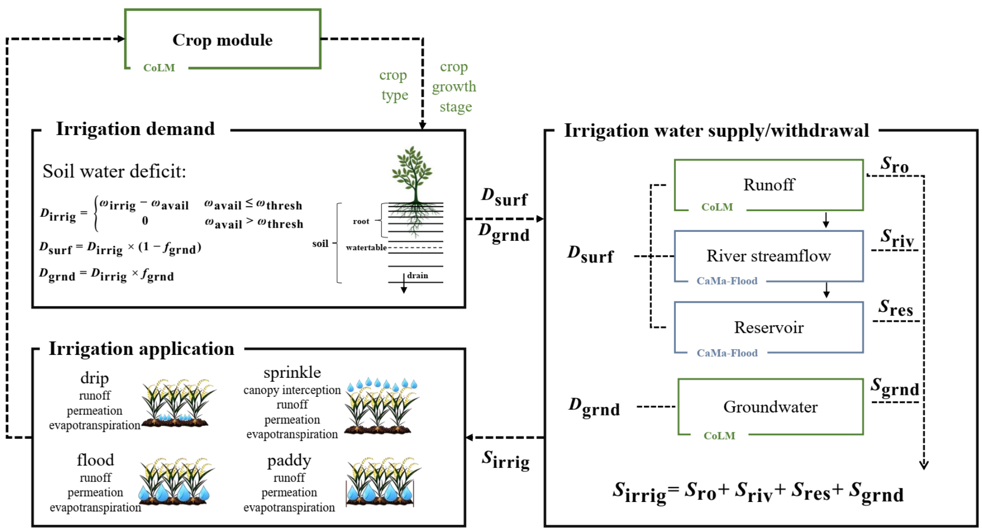

Figure 1. Diagram of the two-way coupled irrigation water system in the Common Land Model.

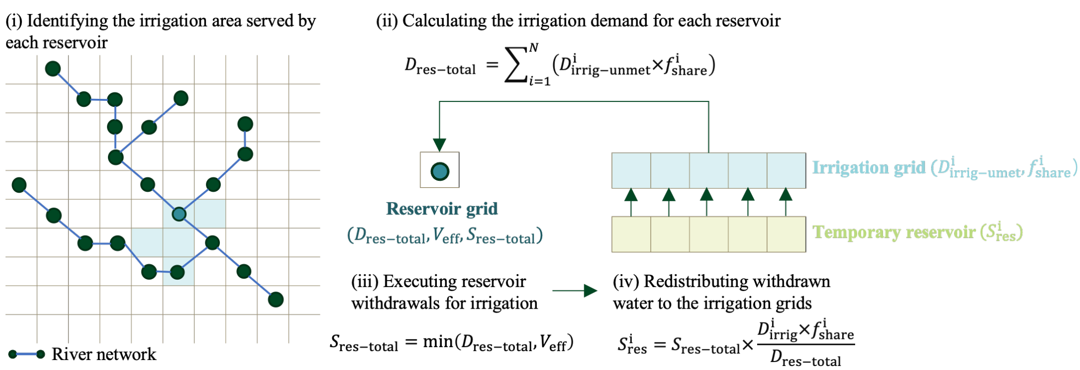

Figure 2. Diagram of the reservoir water supply scheme.

2.2.3.1 Groundwater supply

Groundwater supply is constrained by the availability of water within the aquifer. In CoLM, the groundwater table interacts with soil layers through vertical water exchange, allowing recharge or withdrawal of water from the aquifer (Li et al., 2017). The evolution of the groundwater table is determined by the balance of soil water recharge and subsurface outflow, with the specific yield dynamically linking the water table position to changes in soil moisture and aquifer storage. When irrigation is required, water is directly extracted from the top of the simulated aquifer, and the water table depth is updated accordingly. This process continues until either the irrigation demand is fully met, or the water table falls below a predefined threshold, set as 1 meter below the initial depth at the beginning of the year (Jasechko et al., 2024; Russo and Lall, 2017). Groundwater supply is immediately available upon demand, with no temporal lag

https://doi.org/10.5194/egusphere-2024-4093
Preprint. Discussion started: 22 January 2025

between the request and its availability for irrigation. Changes in the water table depth can then affect subsurface drainage and recharge from the bottom soil layer to the aquifer.

2.3 Materials

2.3.1 Input datasets

In this study, CoLM was implemented across the contiguous United States at a 0.25° spatial resolution for the period 2001–2016. Meteorological input data were derived from the WATCH Forcing Data methodology applied to ERA-Interim data (WFDEI) (Weedon et al., 2014), which has also been utilized in the Inter-Sectoral Impact Model Intercomparison Project Phase 2a (ISIMIP2a; Gosling et al., 2019). Soil property data were sourced from the Global Soil Dataset for Earth System Modeling (GSDE), originally provided at a spatial resolution of 30 arc-seconds (Dai et al., 2019; Shangguan et al., 2014). Land cover data were derived from the MODIS dataset (MCD12Q1; Friedl and Sulla-Menashe, 2022), providing detailed global land classification information at a spatial resolution of 500 meters.

The simulation of irrigation processes also required detailed data on crop areas, planting dates, irrigation areas and irrigation methods. Crop planting areas were derived from the 30-meter resolution CropScape and Cropland Data Layer (CDL) datasets (2008–2020) and aggregated to a spatial resolution of 5 arcminutes for analysis (USDA, 2019). These datasets, produced by the U.S. Department of Agriculture, provide annual, crop-specific land cover information using satellite imagery and ground reference data. For each pixel, we calculated the proportion of cropland relative to the pixel's area (PCT_CROP) and the proportions of maize, wheat, and soybean relative to the cropland area (PCT_CFT). Pixels with a cropland percentage (PCT_CROP) exceeding zero were classified as crop pixels. The Plant Functional Type (PFT) approach employed in CoLM allowed different crops and vegetation types coexist within the same grid cell according to their percentages (PCT_CFT). To define planting and harvesting dates, we utilized an observation-based crop calendar dataset from the Global Gridded Crop Model Intercomparison (GGCMI), which provided information for 20 major crops under both rainfed and irrigated conditions at each grid cell for 1980–2010 (Jägermeyr et al., 2021).

The irrigation map was derived using the 5' resolution data from the FAO Global Map of Irrigation Areas - Version 5 (Siebert et al., 2013). Since the CropScape data does not distinguish between rainfed and irrigated crops, we combined it with the irrigation map to determine the proportions of rainfed and irrigated crops. Irrigation water withdrawals were classified into surface water and groundwater sources following FAO data on regions equipped for groundwater extraction, which informed the allocation of irrigation demand across sources (Siebert et al., 2010). The irrigation application method data was obtained from Yao's global irrigation map, which details irrigation methods (drip, sprinkler, or flood) for 32 crop types, each assigned a single method (Yao et al., 2022). Jägermeyr et al. (2015) originally used a decision tree to refine

https://doi.org/10.5194/egusphere-2024-4093
Preprint. Discussion started: 22 January 2025

AQUASTAT's data, classifying irrigation methods for 14 Crop Functional Types (CFTs) based on crop area, soil characteristics, and socio-economic conditions. Yao et al. (2022) then matched these CFTs to 32 crop types in CLM5 and incorporated an additional irrigation method, *paddy*, specifically for rice-growing regions, creating a more detailed global irrigation dataset.

For river routing simulations in CaMa-Flood, the baseline topography was derived from the Multi-Error-Removed Improved-Terrain Hydrography dataset (MERIT Hydro; Yamazaki et al., 2019). Fundamental information on dams/reservoirs in the river network, including dam name, coordinates, total storage capacity, and drainage area, was obtained from the GRanD database (Lehner et al., 2011). GRanD version 1.3 contains data on 7,320 dams globally, along with their associated reservoirs. The locations of the dams in the 0.25° river map were determined following the method outlined by Hanazaki et al. (2022), which enabled the identification of 1464 reservoirs across the contiguous United States (Figure S2). In addition to GRanD, the Global Reservoir Surface Area Data Set (GRSAD; Zhao and Gao, 2018) and the Global Reservoir Geometry Database (ReGeom; Yigzaw et al., 2018) were used to estimate reservoir parameters, such as storage capacity at emergency, flood control, and critical levels (Hanazaki et al., 2022). GRSAD provides a monthly time series of surface areas for 6,817 GRanD reservoirs from 1984 to 2015, based on global surface water occurrence data (Pekel et al., 2016). ReGeom contains storage-area-depth information for 6,824 reservoirs in GRanD, with geometry estimates derived from assumed surface and cross-sectional shapes, as well as data on reservoir extent, total storage, and surface area.

2.3.2 Validation datasets

To evaluate the scheme developed in this study, we focused on validating irrigation water withdrawal volumes, land fluxes (including energy fluxes and river flows) and crop yields in irrigated areas. We used hydrological survey data from the U.S. Geological Survey (USGS, 2023), which provided detailed statistics on total irrigation water withdrawals, categorized by surface and groundwater sources, every five years since 2000. Within the timeframe of this study, data were available for the years 2005, 2010, and 2015. Building on this, Ruess et al. (2024) employed a global hydrological model (PCR-GLOBWB) to estimate annual, crop-specific irrigation water withdrawals from 2008 to 2020. Additionally, we compared the irrigation water withdrawal volumes simulated by our model with those generated by six other hydrological models—VIC, PCR-GLOBWB, MATSIRO, LPJmL, H08, and DBH—that participated in ISIMIP2a (Gosling et al., 2019). Although more hydrological models were included in ISIMIP2a, our comparison was limited to these six because they provided irrigation water withdrawal outputs. The simulations were driven by the WFDEI climate dataset, with a spatial resolution of 0.5° and covering the period from 1971 to 2010.

For land surface flux validation, we used monthly latent and sensible heat fluxes provided by FLUXCOM at a resolution of 0.5° (Jung et al., 2019). FLUXCOM leveraged FLUXNET site

https://doi.org/10.5194/egusphere-2024-4093
Preprint. Discussion started: 22 January 2025

observations and extended these globally through machine learning algorithms, resulting in a global dataset for latent heat, sensible heat, and carbon fluxes. For temperature validation, we used land surface temperature data from 2001 to 2016 at a spatial resolution of 0.1° from the ERA5-Land reanalysis dataset (Muñoz-Sabater et al., 2021).

For streamflow validation, we utilized monthly streamflow data from the Global Runoff Data Centre (GRDC, 2023) for the period 2001–2016. To ensure robust validation, we excluded catchments with fewer than five years of data during the study period and focused on catchments significantly influenced by irrigation while minimizing the impacts of other anthropogenic activities. These selection criteria ultimately resulted in 77 catchments being included in the analysis (Figure S7).

For crop yield validation, we relied on annual yield reports for irrigated and rainfed crops from the USDA NASS at the county level, which is regarded as a reliable source of yield statistics (USDA/NASS, 2023). The data for irrigated crops primarily covered the Central Plains of the United States, with limited coverage in the eastern and western regions. We aggregated our grid-based yield simulation results to the county level and performed validation only for regions and years with available USDA data.

2.4 Experimental Design

This study conducted three simulation experiments to evaluate the effectiveness of the newly developed module by comparing their performance: (i) Non-Irrigation Experiment (abbreviated as noirrig): This scenario assumes all crops in the region are rainfed, with no irrigation applied. It serves as a baseline to represent natural surface water and energy balance conditions. (ii) Unlimited Irrigation Experiment (abbreviated as noirrig-unlim): This scenario distinguishes between irrigated and rainfed areas based on crop maps. In irrigated areas, crop water demands are fully satisfied throughout the growing season, without considering the limitations of water resources. (iii) Limited Irrigation Experiment (abbreviated as irrig-lim): In this scenario, irrigation water is supplied proportionally from surface water and groundwater based on availability, as illustrated in Figure 1. Here, irrigation is constrained by the availability of surface and groundwater, which may result in unmet crop water demands.

The non-irrigation experiment was first simulated for the period 2001–2010 to stabilize vegetation carbon and nitrogen pools, soil moisture, and the groundwater table. This stabilized state served as the initial condition for all three experiments. The main simulation period spanned 2001-2016, covering the contiguous United States at a spatial resolution of 0.25° × 0.25°. In the subsequent analysis, key evaluation metrics—bias, root-mean-square error (RMSE), Pearson correlation coefficient (r), and Kling-Gupta efficiency (KGE)—were employed to assess the performance of the simulations.

https://doi.org/10.5194/egusphere-2024-4093
Preprint. Discussion started: 22 January 2025

3. Results

3.1 Evaluation of simulated irrigation water withdrawal

3.1.1 Comparison with observations

Based on annual irrigation withdrawal data from the USGS, states in the western and central United States withdraw significantly more water for irrigation than those in the eastern regions (Figure 3a). This is primarily due to the relatively low precipitation in the western and central regions, where the majority of irrigated areas are located, while crops in the eastern U.S. are predominantly rainfed. The top five states with the highest annual irrigation withdrawals—California (CA), Idaho (ID), Colorado (CO), Arkansas (AR), and Montana (MT)—are all situated in the Midwest and West (Figure 3b). Nationally, the total annual irrigation withdrawal averages approximately 166.23 km^3 yr^{-1}, based on data from 2005, 2010 and 2015. In comparison, the irrig-unlim and irrig-lim schemes simulate national total withdrawals of 290.94 km^3 yr^{-1} and 120.81 km^3 yr^{-1}, respectively. As illustrated in Figure 3c-f, the simulations capture the spatial patterns of water withdrawals across different states effectively, with the irrig-lim scheme yielding better performance. The root-mean-square-error (RMSE) and correlation coefficient (r) for the irrig-lim scheme are 3.60 km^3 yr^{-1} and 0.82, respectively, slightly outperforming the corresponding values for the irrig-unlim scheme (9.78 km^3 yr^{-1} and 0.76).

Irrigation water withdrawals draw from both surface water and groundwater sources. According to USGS reports, most irrigation withdrawals in the central U.S. come from groundwater (Dieter et al., 2018). In states such as Missouri (MO), Kansas (KS), Iowa (IA), Illinois (IL), Rhode Island (RI), and Mississippi (MS), the share of groundwater withdrawals exceeds 90% (Figure 4c). In contrast, states with high surface water withdrawals are primarily in the eastern and western U.S., with states like Wyoming (WY), Connecticut (CT), Kentucky (KY), and Montana (MT) reporting surface water withdrawal proportions greater than 90%. These spatial variations in water source usage are primarily attributed to the central U.S.'s abundant groundwater resources and widespread groundwater extraction infrastructure.

In our simulations, the irrig-lim scheme effectively accounts for irrigation water withdrawals from different sources, constrained by their availability. Encouragingly, the scheme generally reproduces observed annual surface water and groundwater withdrawals across states (Figure 4a-b), achieving correlation coefficients of 0.68 and 0.95, respectively. Furthermore, the simulated proportions of water sources closely align with observed data (Figure 4c-d), with a correlation coefficient of 0.64 ($p < 0.01$). However, the model tends to underestimate the surface water withdrawal proportions in the northwestern regions of the U.S. (particularly in Montana and Colorado; Figure 4d), while slightly overestimating them in some central and eastern states. This discrepancy may stem from limitations in the data used to allocate water demand. Specifically, the model relies on pre-determined groundwater extraction infrastructure proportions, which may

https://doi.org/10.5194/egusphere-2024-4093
Preprint. Discussion started: 22 January 2025

not accurately reflect actual extraction practices, particularly as the dataset was published in 2005 and may not account for subsequent changes in groundwater infrastructure in certain states. Alternatively, the discrepancy could arise from model biases in simulating surface and groundwater availability. For example, in the northwestern region, surface runoff is heavily influenced by snowmelt and glacial meltwater (Li et al., 2017), and biases in simulating these processes could lead to an underestimation of surface water availability.

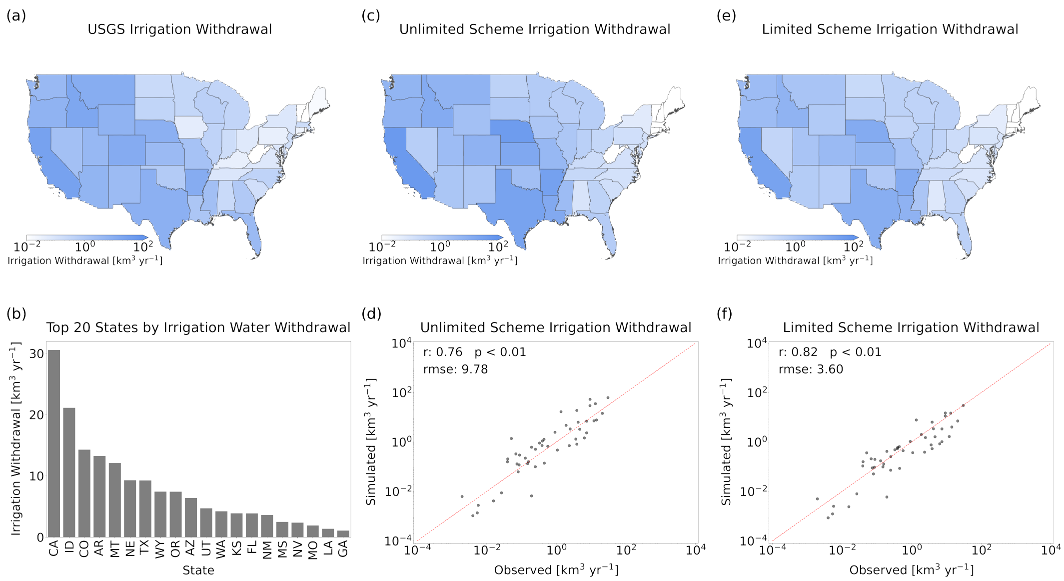

Figure 3. Comparison of reported and simulated irrigation water withdrawal in the United States. (a) Annual irrigation water withdrawal reported by the USGS for individual states. (b) Annual withdrawal amounts for the top 20 states by irrigation water withdrawal. (c) Annual irrigation water withdrawal simulated by CoLM using the unrestricted water supply (irrig-unlim) scheme for individual states. (d) Comparison of reported and simulated irrigation water withdrawal (using the irrig-unlim scheme) for individual states, with Pearson correlation coefficient (*r*) and root mean square error (RMSE) displayed, along with statistical significance (two-tailed Student's t-test). (e) Annual irrigation water withdrawal simulated by CoLM using the restricted water supply (irrig-lim) scheme for individual states. (f) Comparison of reported and simulated irrigation water withdrawal (using the irrig-lim scheme) for individual states.

https://doi.org/10.5194/egusphere-2024-4093
Preprint. Discussion started: 22 January 2025

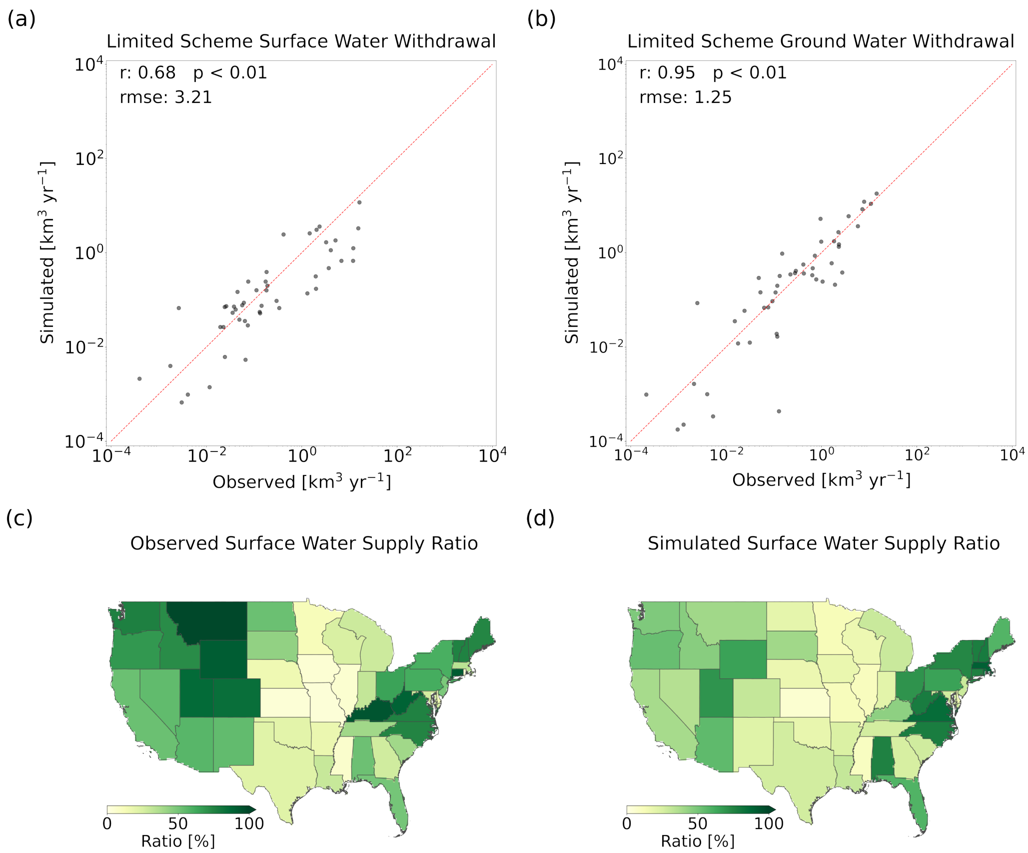

Figure 4. Comparison of reported and simulated irrigation water withdrawal in the United States by water source. (a) Comparison of reported and simulated surface water withdrawal volumes for individual states. (b) Same as (a), but for groundwater withdrawal volumes. (c) Proportion of surface water in irrigation withdrawal, based on USGS reports for individual states. (d) Proportion of surface water in irrigation withdrawal, simulated by CoLM using the irrig-lim scheme for individual states.

Ruess et al. (2024), using data from the USGS and model outputs from PCR-GLOBWB 2, generated an irrigation water withdrawal dataset that included withdrawal volumes for major crops in the U.S. According to this dataset (Figure 5), wheat is the largest consumer of irrigation water, with an average annual withdrawal of approximately 27.29 km^3 yr^{-1}, followed by maize at about 20.91 km^3 yr^{-1}. In contrast, soybean requires considerably less irrigation (i.e., 5.89 km^3 yr^{-1}), partly due to its greater drought tolerance and smaller planted area compared to the other two crops. Under the irrig-unlim (irrig-lim) simulation scheme, the annual irrigation withdrawals for maize, wheat, and soybean are 53.98 km^3 yr^{-1}, 47.53 km^3 yr^{-1}, and 29.99 km^3 yr^{-1} (19.19 km^3 yr^{-1},

https://doi.org/10.5194/egusphere-2024-4093
Preprint. Discussion started: 22 January 2025

17.95 km^3 yr^{-1}, and 11.05 km^3 yr^{-1}), respectively. Once again, the irrig-lim scheme provides a closer alignment with observation-based data, as indicated by a lower RMSE (Figure 5). These results suggest that our irrigation module generally performs well in simulating total national annual water withdrawals, the spatial distribution of withdrawals (Figure 3), the proportion of water source types (Figure 4), and the irrigation volumes for different crops (Figure 5).

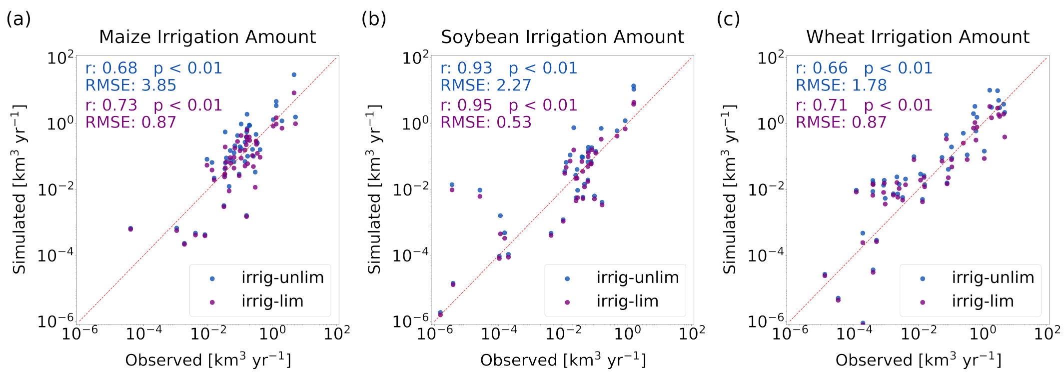

Figure 5. Comparison of reported and simulated irrigation water withdrawal in the United States by crop type. (a) Comparison of reported and simulated irrigation water withdrawal for maize, using both the unrestricted (irrig-unlim, blue dots) and restricted (irrig-lim, purple dots) supply schemes for individual states. (b-c) Same as (a) but for soybean and wheat.

3.1.2 Comparison with other models

We further compare the irrigation water withdrawal simulations from this study with outcomes from six global hydrological models (VIC, PCR-GLOBWB, MATSIRO, LPJmL, H08, and DBH) that participated in ISIMIP2a. Notably, all simulations used the same climate forcing (WFDEI), ensuring consistency in the comparison. Our results, particularly from the irrig-lim scheme, closely align with observed total national annual irrigation withdrawals. By contrast, five of the six models, excluding LPJmL, exhibit larger absolute deviations from observed value (Figure 6a). Regarding spatial distribution, most models perform well (Figure 6b), with LPJmL (orange dots) achieving the highest correlation coefficient (0.89) and the lowest RMSE (2.86 km^3 yr^{-1}). The irrig-lim scheme in this study (purple dots) performs comparably to LPJmL, demonstrating competitive accuracy. In terms of temporal dynamics, comparisons across models are limited due to the scarcity of observed data. However, the general seasonal patterns are consistent across models (Figure S5), with the highest irrigation withdrawals occurring in June and July, and the lowest in January and December. Most models exhibit similar seasonal fluctuations, with irrigation volumes during peak months approximately ten times greater than during off-peak months. Overall, these results suggest that our model performs similarly to, or even better than, existing models in simulating irrigation water withdrawals in the U.S.

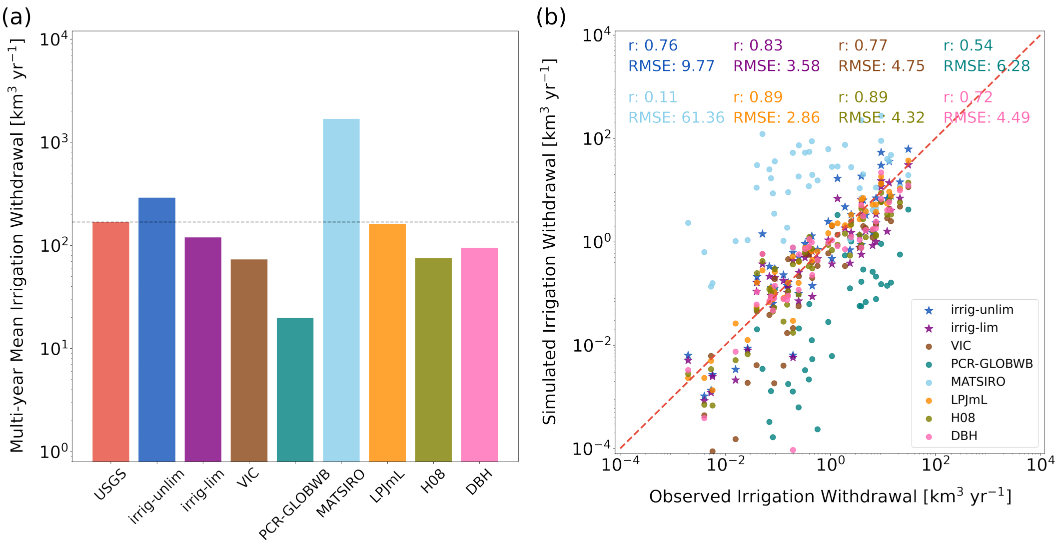

Figure 6. Comparison of irrigation water withdrawal simulated by CoLM and six global hydrological models participating in ISIMIP2a. (a) Annual total irrigation water withdrawal amounts in the United States as reported by the USGS, compared with simulations from CoLM (using both the irrig-unlim and irrig-lim schemes) and the six global hydrological models. (b) Comparison of reported and simulated irrigation water withdrawal for individual states, with Pearson correlation coefficient (*r*) and root mean square error (RMSE) for each simulation displayed.

3.2 Evaluation of simulated land energy and water fluxes

3.2.1 Evaluation of simulated energy fluxes

We evaluate CoLM's performance in simulating surface energy fluxes over irrigated areas in the U.S. using different schemes, with FLUXCOM monthly sensible heat (*SH*) and latent heat (*LH*) fluxes as observational references. Figure 7 compares multi-year monthly averages of observed and simulated *SH* and *LH* fluxes across irrigated grid points. Without irrigation (the noirrig scheme), the model significantly overestimates *SH* (Figure 7a) with an average bias of 16.89 W m^{-2} (44.53%) and underestimates *LH* (Figure 7c) with an average bias of 18.84 W m^{-2} (37.11%). In contrast, biases over non-irrigated grids are considerably lower, at 3.04% and 17.38% for *SH* and *LH*, respectively (Figure S6). This indicates that CoLM performs satisfactorily in simulating energy processes over natural vegetation and rainfed areas, but less so over irrigated regions.

Upon introducing the irrigation module, the simulation errors in surface energy fluxes over irrigated areas are significantly reduced. Under the irrig-unlim and irrig-lim schemes, average *SH* biases decrease to 27.10% and 30.79%, respectively, while *LH* biases decrease to 18.41% and

https://doi.org/10.5194/egusphere-2024-4093
Preprint. Discussion started: 22 January 2025

22.18%. These improvements are evident across most irrigated grid points, as illustrated by the KDE curves of KGE, which indicate an increase in grid points with higher KGE values (Figure 7). A KS test confirms that the differences between the irrigation (i.e., the irrig-unlim and irrig-lim schemes) and noirrig simulations are statistically significant. Although the irrig-unlim scheme performs slightly better than irrig-lim for *SH* and *LH*, this difference is not significant.

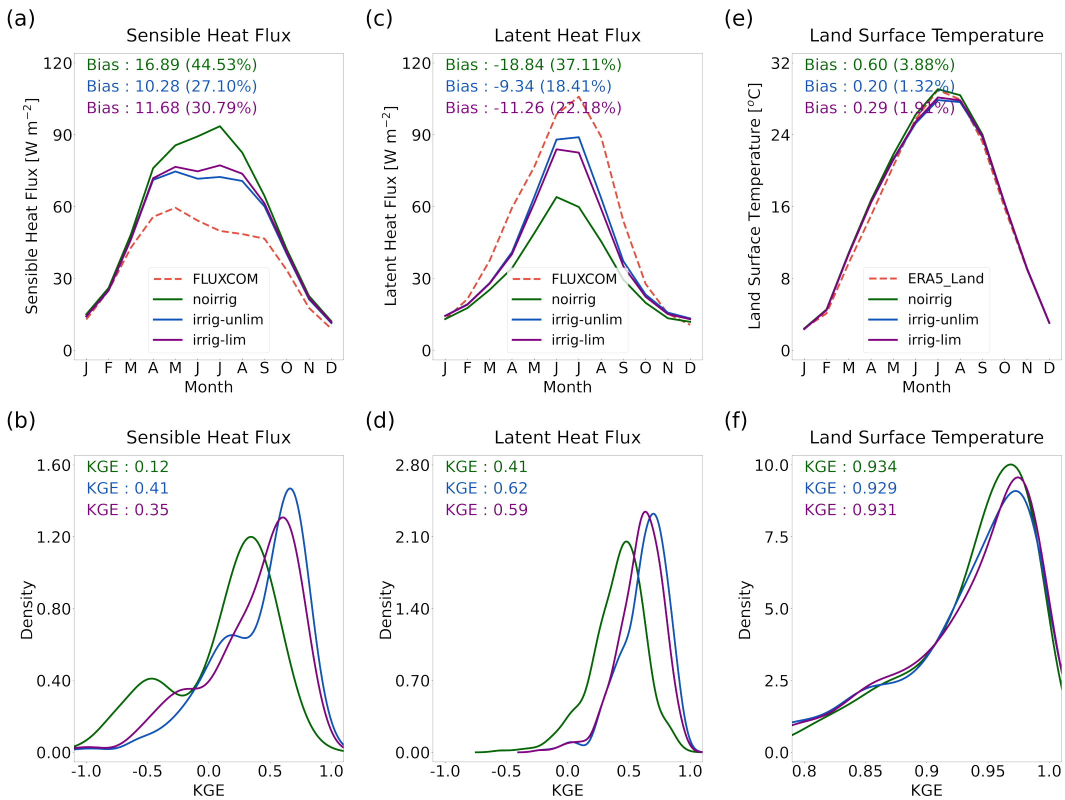

Figure 7. Evaluation of simulated energy fluxes and land surface temperature in the irrigation region. (a) Monthly sensible heat flux averaged from 2001 to 2016, based on FLUXCOM dataset and simulated by CoLM using the noirrig, irrig-unlim, and irrig-lim schemes in irrigation regions of the United States, with the bias between simulations and observations (i.e., FLUXCOM) indicated in the panel. (b) Kernel density estimate (KDE) curves for the Kling-Gupta efficiency (KGE) between observed and simulated monthly sensible heat flux for each irrigation grid, with mean KGE value indicated in the panel. (c-d) Same as (a-b) but for latent heat flux. (e-f) Same as (a-b) but for land surface temperature, using data from ERA5-Land reanalysis dataset.

Additionally, the FLUXCOM data (red dashed line) show that the highest monthly *SH* and *LH* occur in May and July, respectively. However, the noirrig simulation (green solid line) fails to capture this seasonal peak, showing instead that *SH* peaks in July and *LH* in June. This

https://doi.org/10.5194/egusphere-2024-4093
Preprint. Discussion started: 22 January 2025

discrepancy is not present in non-irrigated areas (Figure S6), suggesting that irrigation in agricultural regions (and the subsequent crop growth it supports) substantially affects the seasonal pattern of regional energy balance. When the irrigation module is incorporated into the model, these seasonal patterns are more accurately reproduced, with the timing of the simulated peak months aligning more closely with FLUXCOM data (blue and purple solid lines).

The incorporation of the irrigation module improves the simulation of energy partitioning in irrigated areas, enabling the model to better capture surface temperature dynamics (Figure 7e). Under the noirrig scheme, the average bias of monthly surface temperature is 0.6℃ (3.88%). This bias decreases to 0.20℃ (1.32%) with the irrig-unlim scheme and 0.29℃ (1.91%) with the irrig-lim scheme. However, even with irrigation included, the simulated total evapotranspiration remains systematically underestimated (Figure 7c). This underestimation is also evident in non-crop areas (Figure S6c), suggesting that it may not be due to limitations in the irrigation module itself but rather to certain deficiencies in CoLM's evapotranspiration simulation approach.

3.2.2 Evaluation of simulated river flow

Irrigation processes can significantly alter natural hydrological dynamics and river flow patterns both temporally and spatially. To evaluate the effectiveness of the irrigation module in capturing these impacts, we compare model outputs with observed catchment streamflow data. We select catchments that are substantially influenced by irrigation while minimizing the effects of other anthropogenic activities. Figure S7 illustrates the locations of the selected 77 catchments. Figure 8 shows that CoLM's performance in simulating runoff—and consequently streamflow—remains limited, with relatively low average KGE values across all three schemes. This limitation is likely due to the use of a simplified runoff parameterization scheme in CoLM (Li et al., 2011). However, it is encouraging to note that the irrig-lim scheme notably improves monthly streamflow simulations compared to the noirrig scheme, increasing the average KGE from -0.57 to -0.49 and reducing the average percentage bias (PBIAS) from 117.28% to 106.54%. The enhancement can be largely attributed to the incorporation of irrigation effects, which account for reduced streamflow due to increased water use for evapotranspiration. This adjustment effectively mitigates the overestimation of streamflow observed in the noirrig scheme.

Furthermore, our analysis reveals that the irrig-unlim scheme significantly reduces the accuracy of streamflow simulations compared to the noirrig scheme, leading to a pronounced overestimation of river discharge. The average relative bias increases substantially from 117.28% to 147.23% (Figure 8b). This issue arises because the irrig-unlim scheme meets any irrigation demand by introducing additional water directly into the system without considering its source. Such an approach is common among crop and land surface models that incorporate irrigation (Malek et al., 2017; Yao et al., 2022; Zhang et al., 2020b). However, our findings indicate that introducing extra water for irrigation without accounting for its specific sources and limitations may lead to an imbalance in the water budget from a comprehensive perspective of the entire

https://doi.org/10.5194/egusphere-2024-4093
Preprint. Discussion started: 22 January 2025

water system, undermining the model's ability to accurately represent the dynamics of the hydrological system.

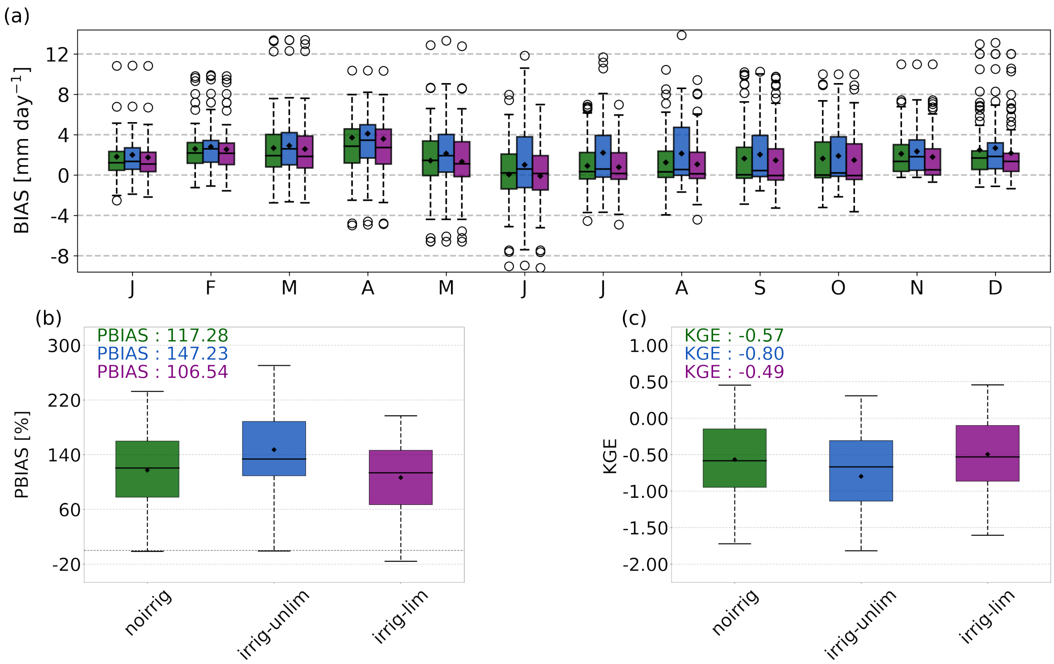

Figure 8. Evaluation of simulated streamflow in 77 irrigation-affected catchments. (a) Multi-year average monthly streamflow bias simulated using the noirrig, irrig-unlim, and irrig-lim schemes in the evaluation catchments. The boxes represent the interquartile range, black lines indicate median values, black dots show mean values, and dashed black whiskers extend to 1.5 times the interquartile range; points outside the boxes represent outliers. (b) Percentage bias (PBIAS) between observed monthly streamflow and simulations from CoLM under the noirrig, irrig-unlim, and irrig-lim schemes, with the average PBIAS value indicated in the panel. (c) Same as (b) but for the Kling-Gupta efficiency (KGE) between simulated and observed streamflow.

3.3 Evaluation of simulated crop yield

Irrigation reflects a direct human influence on crop yields by providing supplemental water. Crop models primarily focus on this aspect, but they often neglect how irrigation affects other processes. Conversely, most hydrological models concentrate on the impact of irrigation withdrawals on the water cycle, with some also addressing energy fluxes, yet pay less attention to crop yield. From this perspective, land surface models offer distinct advantages; they provide a more detailed representation of hydrological and surface energy processes compared to crop

https://doi.org/10.5194/egusphere-2024-4093
Preprint. Discussion started: 22 January 2025

models, while also presenting more physics-based representations of crop growth than traditional hydrological models. Therefore, this study further evaluates whether incorporating the developed irrigation module can enhance crop yield the simulations.

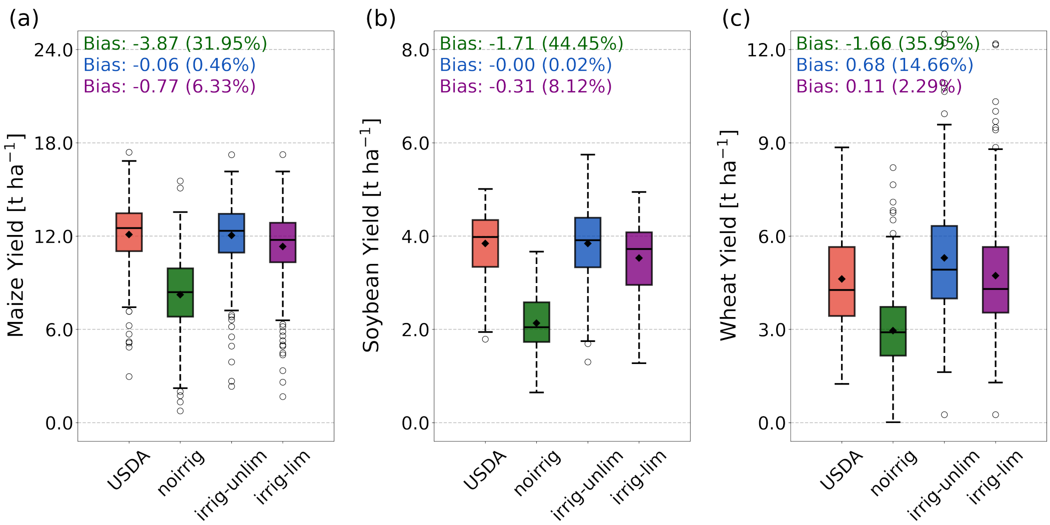

Figure 9. Evaluation of crop yield simulated using different schemes in the United States. (a) Maize yield in irrigated maize-growing regions of the United States, as reported by the USDA (orange boxes), compared with simulations by CoLM using the noirrig (green boxes), irrig-unlim (blue boxes), and irrig-lim (purple boxes) schemes. Since reported yields are at the county scale, grid-based simulation results were aggregated to corresponding counties. (b-c) Same as (a) but for soybean and wheat yields.

Using county-scale crop yield data for irrigated and rainfed regions provided by the USDA, we assess simulated yields under both irrigated and non-irrigated scenarios. The dataset may not comprehensively cover all irrigated areas in the U.S. or all years during the study period, so comparisons are limited to regions and years with reported data. In rainfed regions, the model broadly reproduces average annual yields for the maize, soybean, and wheat (Figure S8). However, in irrigated regions, the model without irrigation significantly underestimates crop yields, with average underestimations of 31.95%, 44.45%, and 35.95% for maize, soybean, and wheat, respectively (Figure 9). Under both the irrig-umlim and irrig-lim schemes, despite slight differences in performance across crops, the model effectively simulates yield increases under irrigation, aligning well with observations. Differences between the two irrigation schemes are minimal: the irrig-unlim scheme performs slightly better for maize and soybean in terms of average biases, while the irrig-lim scheme shows better performance for wheat.

Furthermore, based on limited annual yield data, we observe that considering irrigation generally improves the model's ability to capture inter-annual yield fluctuations (Figure S9). The KGE of

https://doi.org/10.5194/egusphere-2024-4093
Preprint. Discussion started: 22 January 2025

annual yields under the noirrig scheme are -1.342, -1.451, and -1.308 for maize, soybean, and wheat, respectively, while with the irrig-umlim and irrig-lim schemes, the KGE values increase to 0.101, -1.132, and 0.197, and -0.158, -1.449, and -0.144, respectively.

4. Discussions

4.1 Applications of the developed module

4.1.1 Impacts of irrigation on energy budget

Numerous studies have highlighted the impacts of irrigation on global and regional energy budgets and near-surface climates. In this study, we similarly examine the effects of irrigation on the energy budget over irrigated areas in the U.S. by comparing results from the irrig-lim and noirrig scheme. Consistent with prior research, we find that irrigation increases latent heat (*LH*) by 7.53 W m^{-2} (23.25 %) and decreases sensible heat (*SH*) by 5.18 W m^{-2} (9.48 %) averaged from 2001 to 2016, resulting in an approximately 0.30°C reduction in land surface temperature (Figure 10). Since land-atmosphere coupling is not included, the primary mechanisms driving these impacts are increased soil evaporation due to enhanced soil moisture and greater vegetation transpiration driven by improved crop growth following irrigation (Figure S10 a-b). Annually, these mechanisms contribute roughly equally to the increase in total evapotranspiration in irrigated regions, with pronounced seasonal differences: during the peak growing seasons (summer and autumn), the contribution was dominated by vegetation transpiration, while in other seasons, particularly winter, the increase in soil evaporation plays a larger role in affecting regional energy distribution and temperature (Figure S10c).

This study further explores the spatial characteristics of these impacts, analyzing the correlations between irrigated area, irrigation water withdrawal, and changes in *LH*, *SH*, and land surface temperature (ΔLH, ΔSH, ΔT_s) across different climate zones. Notably, irrigation has the most substantial impact in arid regions, especially on *LH*, where ΔLH is more than double that of semi-arid and humid regions, with a larger reduction in temperature by 0.36°C. Interestingly, while previous studies have emphasized irrigated area as the primary determinant of irrigation-induced climate effects (Al-Yaari et al., 2022; Chen and Dirmeyer, 2019), our results indicate that irrigation water withdrawal has a stronger influence on the regional energy budget and temperature. Across all climate zones, ΔSH, ΔLH, and ΔT_s are significantly correlated ($p < 0.01$) with irrigation water withdrawal, with correlation coefficients of -0.81, 0.79, and -0.82, respectively (Figure 10 (b, e and h)), which are higher than the correlations with irrigated area (-0.59, 0.61, and -0.52; Figure 10 (c, f and i)). This emphasizes the critical role of water availability in modulating the climate effects of irrigation.

https://doi.org/10.5194/egusphere-2024-4093
Preprint. Discussion started: 22 January 2025

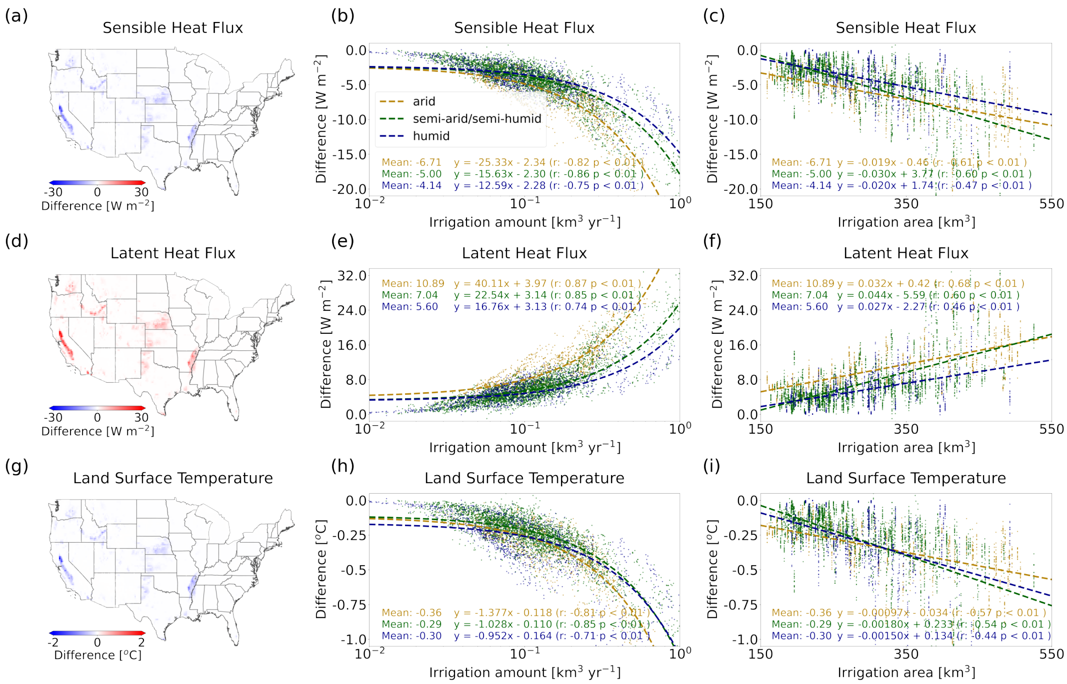

Figure 10. Impact of irrigation on local energy flux and surface temperature in the United States. (a) Impact of irrigation on sensible heat flux, quantified by the difference (ΔSH) between the noirrig and irrig-lim simulation results. (b) Relationship between irrigation amount and ΔSH, with grid colors indicating the climate zones (i.e., arid, semi-arid/semi-humid, humid). For each climate zone, the mean ΔSH, the regression line of irrigation amount versus ΔSH, and the regression equation are displayed. (c) Same as (b), but for the relationship between irrigation area and ΔSH. (d-f) Same as (a-c), but for the impact on latent heat flux (ΔLH). (g-i) Same as (a-c), but for the impact on land surface temperature (ΔT_s).

It is important to note that this study employs offline land simulations and does not account for land-atmosphere interactions, which may introduce biases in the estimated climate impacts. Future studies should include coupled land-atmosphere simulations to provide a more comprehensive assessment (Cook et al., 2015; Puma and Cook, 2010; Sacks et al., 2009). Another aspect worth considering is that some farmers irrigate not only to address water deficits but also to mitigate heat stress during high-temperature periods (Verma et al., 2020). This practice can notably affect local temperatures. For instance, surface water temperatures generally track air temperatures, whereas groundwater temperatures remain relatively stable throughout the year—typically warmer than air in winter and cooler in summer. This temperature difference, especially in regions relying on groundwater irrigation, may have non-negligible effects on local climate that should be incorporated into future modeling efforts.

https://doi.org/10.5194/egusphere-2024-4093
Preprint. Discussion started: 22 January 2025

4.1.2 Assessments of irrigation water security

This study compares the irrigation schemes with and without water availability constraints, highlighting the necessity and importance of incorporating water limitations into simulations. Our results demonstrate that including these constraints improves simulation accuracy, particularly in the modeling of water systems. Specifically, irrigation water withdrawal simulated under the irrig-lim scheme aligns more closely with observational data (Figure 3 and Figure 6). Validation against river flow observations further supports the improved performance of the irrig-lim scheme. Importantly, this scheme avoids the risk of potential water imbalances in the modeled hydrological system—an issue commonly associated with non-constrained schemes (Figure 8).

Additionally, incorporating water availability constraints more accurately reflects the reality of water resource utilization. By accounting for the interconnections between subsystems within the irrigation water demand-supply system, this approach enables simulation and prediction of irrigation water security issues. Here, we visualize the average number of days when water supply was insufficient to fully meet irrigation demand that simulated by the irrig-lim scheme (Figure 11). Spatially, in humid regions, where irrigation demand is low and water resources are abundant, fewer days of unmet irrigation needs occur. Conversely, in arid regions, where irrigation demand is high and water resources are often limited, the number of unmet irrigation days increases significantly. Figure 11a illustrates that states with a higher number of unmet irrigation days are also those with relatively scarce water resources (e.g., Montana and Nevada). From a temporal perspective, drought years lead to increased irrigation requirements due to reduced precipitation or higher evaporative demand. Although additional water withdrawals can partially address this increased demand, drought conditions often simultaneously result in deficits in both surface and groundwater resources within the water system. As a result, most states experience a substantial increase in unmet irrigation days during drought years (an average of 43 days). In contrast, during wetter years, the number of unmet days decreases significantly (an average of 31 days).

Reported disaster data show that even with irrigation, significant crop losses can occur during drought years, aligning with broader water security challenges (Mieno et al., 2024). Our approach effectively captures this phenomenon by describing the connectivity between subsystems in the water demand-supply system and highlighting the impact of water limitations on irrigation. In contrast, ignoring these constraints risks underestimating potential food security issues in a future characterized by more frequent and/or severe droughts. This represents a critical limitation of crop and land surface models that adopt irrigation schemes without considering water availability constraints.

https://doi.org/10.5194/egusphere-2024-4093
Preprint. Discussion started: 22 January 2025

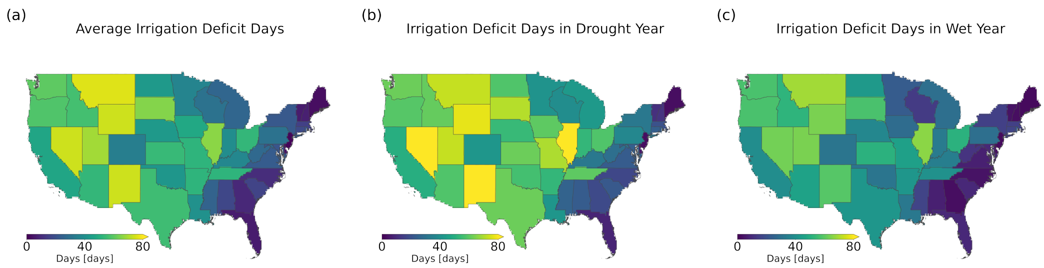

Figure 11. Days per year with unmet irrigation demand (i.e., irrigation deficit days) in the United States simulated by the irrig-lim scheme. (a) Multi-year average irrigation deficit days from 2001 to 2015 for individual states. (b) Irrigation deficit days in drought year for individual states. (c) Irrigation deficit days in wet year for individual states. Drought year (wet year) is defined as the year with the lowest (highest) annual precipitation during 2001–2016.

4.2 Limitations and a way forward

While the developed module represents a significant advancement in modeling irrigation water system within land surface models by providing a comprehensive representation of the irrigation processes—including water demand, water withdrawal, and water utilization, several limitations and assumptions should be acknowledged.

Irrigation water demand in this study is estimated using a soil moisture deficit method. However, the parameterization of certain key variables (e.g., target and threshold soil moisture levels) is overly simplified and does not account for variations among crop types. These parameters are adjustable, and their calibration could further enhance the model's accuracy in reproducing irrigation water use. Additionally, in some cases, farmers irrigate not only to address soil moisture deficits but also to reduce crop heat stress during high-temperature periods—a factor that should be incorporated into future modeling efforts. Furthermore, this study did not account for water losses during conveyance and application. Irrigation losses, as noted by Jägermeyr et al. (2015), include conveyance losses and on-field application losses. By ignoring conveyance losses, the model assumes that water withdrawn equals water applied, likely leading to an underestimation of total irrigation water use. Field application losses depend on irrigation methods (Leng et al., 2017), and while this study considered four irrigation systems with differentiated efficiencies, the reliance on simplified rules and a coarse irrigation map fails to reflect the diversity of irrigation methods and distributions. For example, actual sprinkler systems distribute water in specific spray patterns rather than uniformly. However, the model assumes uniform water distribution across each Crop Functional Type (CFT). Future models could benefit from parameterizations that capture spatial heterogeneity in irrigation distribution (Jägermeyr et al., 2015; Merriam et al., 1999). Moreover, irrigation water demand also depends on agricultural practices, such as crop types, cropping calendars, and planting intensities. While the model determines crop phenology based on meteorological data, real cropping calendars are

https://doi.org/10.5194/egusphere-2024-4093
Preprint. Discussion started: 22 January 2025

influenced by farmers' decisions (Sacks et al., 2010). Incorporating satellite-derived phenology data could better represent these human factors. Addressing these agricultural practices is crucial for improving the accuracy and applicability of irrigation models.

In simulations of irrigation water withdrawal, this study provides a detailed representation of reservoir water withdrawal but acknowledges several sources of uncertainty: First, the dataset includes fewer dams than exist, as it focuses primarily on large dams and may lack data due to protection policies. This omission likely contributes to the underestimation of surface water extraction in some states. Second, all dams are assumed to supply irrigation water, although some reservoirs may not serve this purpose. The irrigation areas served by each dam are unknown, and a generalized estimation method is employed in this study, introducing large uncertainties that remain difficult to validate. Third, dam operations are simplified, while in reality, they often involve complex considerations, such as multi-objective operations and coordinated management of multiple reservoirs. Advanced reservoir optimization strategies, which require predictive simulations and prior knowledge of future inflows and demands, are not incorporated into the model, presenting a significant challenge for considering the impacts of complex human decision-making in land surface models.

Determining the division of irrigation water withdrawals between surface and groundwater sources, as well as the withdrawal sequence, is also critical. This study allocates irrigation demand based on pre-defined proportions and simultaneously withdraws water from both sources. Surface water demand is met sequentially through local runoff, river discharge, and upstream reservoir storages. This method, employed in models such as ORCHIDEE v2.2 (Arboleda-Obando et al., 2024) and E3SM (Zhou et al., 2020), provides satisfactory simulations of water source allocation for irrigation (Figure 4 vs. Figure S11). However, its reliability depends on the accuracy of input data and may underestimate withdrawals if any water source is inadequately represented. Alternatively, some models (e.g., MATSIRO and CLM5; Pokhrel et al., 2012; Yao et al., 2022) do not pre-allocate demand but set a fixed order of water withdrawals—typically prioritizing surface water before groundwater. This method tends to satisfy more irrigation demand and provides better estimates in regions with unreported groundwater extraction. We propose that a hybrid approach, defining surface and groundwater proportions dynamically, warrants consideration in future study. For instance, during wet seasons, surface water extraction proportions could increase to reduce groundwater reliance and associated pumping costs. Conversely, during dry seasons, surface water may be more constrained, necessitating greater reliance on groundwater for irrigation. However, such an approach still needs to address challenges, including unreported groundwater use, data scarcity, and the physical, technical, and socio-economic constraints on groundwater use across regions.

Additionally, this study does not account for restrictions beyond water availability, such as local regulations governing water allocation, including water rights and inter-basin water transfers. Alternative water sources, such as desalinated seawater and treated wastewater, also warrant consideration (Vliet et al., 2021). Recent assessments indicate that these unconventional water

https://doi.org/10.5194/egusphere-2024-4093
Preprint. Discussion started: 22 January 2025

sources are experiencing exponential growth (Jones et al., 2019). Although their contributions remain low globally, they play a significant role in water-scarce regions. Incorporating these factors into models could further improve simulations of irrigation water security.

Finally, the developed module's results and applicability are strongly influenced by the CoLM framework itself. A critical aspect requiring careful consideration is the evaluation and calibration of hydrological variables, such as soil moisture, runoff, river discharge, and groundwater levels, which are essential for water resource modeling. Currently, the CoLM employs the simplified top model (SIMTOP) developed by Niu et al. (2005) for runoff simulations. The excessive simplification of this approach, coupled with the lack of calibration, limits the model's accuracy in runoff simulations. Inadequate representation of snow and glacial melt processes introduces regional biases, particularly in northern and midwestern U.S. states where these factors are pivotal. For instance, surface water extraction is underestimated in some states within these regions, likely because the model fails to accurately capture snowmelt and glacial melt contributions to streamflow, leading to erroneous estimates of surface water availability. Similarly, simulated evapotranspiration is systematically underestimated, even in areas without crops or irrigation, likely due to more complex underlying causes. These biases, when aggregated at the watershed level, result in significant discrepancies in river discharge, thereby constraining the model's applicability for water resource management and its ability to predict irrigation water security. Addressing these issues requires urgent improvements in the representation of related processes, along with further calibration and parameter tuning.

5. Conclusions

The growing challenges posed by increasing global food demand and water scarcity underscore the need for advanced modeling tools capable of accurately capturing human-water interactions. This study contributes to addressing this need by implementing a two-way coupled irrigation water system within the Common Land Model. The developed module provides a comprehensive representation of the entire irrigation water use process, including water demand, withdrawal, and utilization. It introduces a refined multi-source water withdrawal framework and achieves bidirectional coupling between water demand and withdrawal during simulation.

The robustness of the new irrigation module is validated through simulations across the contiguous United States, focusing on regional-scale water, energy, and crop yield dynamics. The module effectively simulates total national annual irrigation withdrawals, their spatial distribution, the proportions of different water sources, and irrigation volumes for various crops. Compared to other hydrological models in ISIMIP2a, our model performs similarly or better in simulating U.S. irrigation withdrawals. Incorporating the new irrigation module also significantly improves the accuracy of simulated surface energy fluxes, both in magnitude and seasonal patterns, resulting in more accurate surface temperature predictions. For streamflow, the irrigation scheme accounting for water availability constraints enhances the model's representation of hydrological system dynamics, whereas the unrestricted irrigation scheme introduces potential water budget imbalances. Additionally, the new module markedly improves the model's ability to simulate annual yields and interannual fluctuations of major crops, including maize, soybean, and wheat.

We further apply the developed module in two novel analyses. First, the scheme effectively characterizes the climatic impacts of irrigation, revealing a stronger positive correlation between irrigation water volume, rather than irrigated area, and the intensity of irrigation-induced climatic effects. This highlights the critical role of water availability in modulating irrigation-driven climate impacts. Although more accurate simulation of these effects requires land-atmosphere coupled modeling, the enhanced CoLM is clearly ready for such tasks. Second, the module captures irrigation-related water security issues, particularly during drought years, where water shortages across the resource system lead to irrigation water deficits and associated food security challenges. These results demonstrate the promise of CoLM as a valuable tool for future water use and scarcity assessments, paralleling the functionality of global hydrological models and contributing to initiatives such as the Inter-Sectoral Impact Model Intercomparison Project.

Data Availability Statement

The meteorological variables from the WFDEI can be freely accessed from ftp://rfdata:forceDATA@ftp.iiasa.ac.at. The land cover type datasets (MCD12Q1) can be freely accessed from https://lpdaac.usgs.gov/products/mcd12q1v061/. The soil characteristics datasets (GSDE) can be freely accessed from http://globalchange.bnu.edu.cn/research/data/. The CropScape and Cropland Data Layer (CDL) datasets can be freely accessed from https://nassgeodata.gmu.edu/CropScape/. The crop calendar datasets can be freely accessed from https://zenodo.org/records/5062513/. The irrigation map and irrigation equipment percentage can be freely accessed from https://www.fao.org/aquastat/en/geospatial-information/global-maps-irrigated-areas/latest-version/. The GRanD database can be freely accessed from https://www.globaldamwatch.org/grand/. The GRSAD database can be freely accessed from https://dataverse.tdl.org/dataset.xhtml?persistentId=doi:10.18738/T8/DF80WG/. The ReGeom database can be freely accessed from https://zenodo.org/records/1322884/. The USGS's hydrological survey data can be freely accessed from https://water.usgs.gov/watuse/data/. The USDA NASS's agricultural survey data can be freely accessed from https://quickstats.nass.usda.gov/. The crop-specific irrigation water withdrawals data can be freely accessed from https://doi.org/10.13012/B2IDB-2656127_V1/. The ISIMIP2a datasets can be freely accessed from https://data.isimip.org/search/. The FluxCom datasets can be freely accessed via ftp.bgc-jena.mpg.de. The ERA5-Land skin temperature data can be freely accessed from https://cds.climate.copernicus.eu/datasets/reanalysis-era5-land-monthly-means?tab=download/. The streamflow data (GRDC) can be freely accessed from https://www.bafg.de/GRDC/EN/Home/. CoLM codes are available for download from GitHub (https://github.com/CoLM-SYSU/CoLM202X/).

Author contributions

SZ and YD conceptualized and designed the study. SZ and HL collected the data, developed the model, and conducted the analyses. FL and XL provided assistance with model development. HL prepared the figures. SZ drafted the manuscript. All authors contributed to result interpretation and reviewed the final manuscript.

Competing interests

The authors declare no competing interests.

Acknowledgments

This research was supported by the Guangdong Major Project of Basic and Applied Basic Research (Grant No. 2021B0301030007), the National Natural Science Foundation of China (Grant Nos. 42088101 & 42175168), the Guangdong Natural Science Foundation (Grant No. 2023A1515011541), the Innovation Group Project of Southern Marine Science and Engineering Guangdong Laboratory (Zhuhai) (Grant No. 311022006) and the Fundamental Research Funds for the Central Universities, Sun Yat- sen University (Grant No. 241gqb007). We also acknowledge the high-performance computing support from the School of Atmospheric Science of Sun Yat-sen University.

References

Abdullah, K. bin: Use of water and land for food security and environmental sustainability, Irrigation and Drainage, 55, 219–222, https://doi.org/10.1002/ird.254, 2006.

Al-Yaari, A., Ducharne, A., Thiery, W., Cheruy, F., and Lawrence, D.: The Role of Irrigation Expansion on Historical Climate Change: Insights From CMIP6, Earth's Future, 10, e2022EF002859, https://doi.org/10.1029/2022EF002859, 2022.

Arboleda-Obando, P. F., Ducharne, A., Yin, Z., and Ciais, P.: Validation of a new global irrigation scheme in the land surface model ORCHIDEE v2.2, Geoscientific Model Development, 17, 2141–2164, https://doi.org/10.5194/gmd-17-2141-2024, 2024.

Ball, J. T., Woodrow, I. E., and Berry, J. A.: A Model Predicting Stomatal Conductance and its Contribution to the Control of Photosynthesis under Different Environmental Conditions, in: Progress in Photosynthesis Research, edited by: Biggins, J., Springer, Dordrecht, Netherlands, 221–224, https://doi.org/10.1007/978-94-017-0519-6_48, 1987.

Biemans, H., Haddeland, I., Kabat, P., Ludwig, F., Hutjes, R. W. A., Heinke, J., von Bloh, W., and Gerten, D.: Impact of reservoirs on river discharge and irrigation water supply during the 20th century, Water Resources Research, 47, https://doi.org/10.1029/2009WR008929, 2011.

Blyth, E. M., Arora, V. K., Clark, D. B., Dadson, S. J., De Kauwe, M. G., Lawrence, D. M., Melton, J. R., Pongratz, J., Turton, R. H., Yoshimura, K., and Yuan, H.: Advances in Land

https://doi.org/10.5194/egusphere-2024-4093
Preprint. Discussion started: 22 January 2025

Surface Modelling, Current Climate Change Reports, 7, 45–71, https://doi.org/10.1007/s40641-021-00171-5, 2021.

Bonan, B.: A Land Surface Model (LSM Version 1.0) for Ecological, Hydrological, and Atmospheric Studies: Technical Description and User's Guide, University Corporation for Atmospheric Research, https://doi.org/10.5065/D6DF6P5X, 1996.

Campbell, B., Beare, D., Bennett, E., Hall-Spencer, J., Ingram, J., Jaramillo, F., Ortiz, R., Ramankutty, N., Sayer, J., and Shindell, D.: Agriculture production as a major driver of the Earth system exceeding planetary boundaries, Ecology and Society, 22, https://doi.org/10.5751/ES-09595-220408, 2017.

Chen, L. and Dirmeyer, P. A.: Global observed and modelled impacts of irrigation on surface temperature, International Journal of Climatology, 39, 2587–2600, https://doi.org/10.1002/joc.5973, 2019.

Collatz, G. J., Ball, J. T., Grivet, C., and Berry, J. A.: Physiological and environmental regulation of stomatal conductance, photosynthesis and transpiration: a model that includes a laminar boundary layer, Agricultural and Forest Meteorology, 54, 107–136, https://doi.org/10.1016/0168-1923(91)90002-8, 1991.

Collatz, G. J., Ribas-Carbo, M., and Berry, J. A.: Coupled Photosynthesis-Stomatal Conductance Model for Leaves of C4 Plants, Functional Plant Biology, 19, 519–538, https://doi.org/10.1071/pp9920519, 1992.

Cook, B. I., Shukla, S. P., Puma, M. J., and Nazarenko, L. S.: Irrigation as an historical climate forcing, Climate Dynamics, 44, 1715–1730, https://doi.org/10.1007/s00382-014-2204-7, 2015.

Dai, Y. and Zeng, Q.: A land surface model (IAP94) for climate studies part I: Formulation and validation in off-line experiments, Advances in Atmospheric Sciences, 14, 433–460, https://doi.org/10.1007/s00376-997-0063-4, 1997.

Dai, Y., Zeng, X., Dickinson, R. E., Baker, I., Bonan, G. B., Bosilovich, M. G., Denning, A. S., Dirmeyer, P. A., Houser, P. R., Niu, G., Oleson, K. W., Schlosser, C. A., and Yang, Z.-L.: The Common Land Model, Bulletin of the American Meteorological Society, 84, 1013–1024, https://doi.org/10.1175/BAMS-84-8-1013, 2003.

Dai, Y., Xin, Q., Wei, N., Zhang, Y., Shangguan, W., Yuan, H., Zhang, S., Liu, S., and Lu, X.: A Global High-Resolution Data Set of Soil Hydraulic and Thermal Properties for Land Surface Modeling, Journal of Advances in Modeling Earth Systems, 11, 2996–3023, https://doi.org/10.1029/2019MS001784, 2019.

Dickinson, E., Henderson-Sellers, A., and Kennedy, J.: Biosphere-atmosphere Transfer Scheme (BATS) Version 1e as Coupled to the NCAR Community Climate Model, University Corporation for Atmospheric Research, https://doi.org/10.5065/D67W6959, 1993.

Dieter, C. A., Maupin, M. A., Caldwell, R. R., Harris, M. A., Ivahnenko, T. I., Lovelace, J. K., Barber, N. L., and Linsey, K. S.: Estimated use of water in the United States in 2015, Circular, U.S. Geological Survey, https://doi.org/10.3133/cir1441, 2018.

https://doi.org/10.5194/egusphere-2024-4093
Preprint. Discussion started: 22 January 2025

Döll, P., Müller Schmied, H., Schuh, C., Portmann, F. T., and Eicker, A.: Global-scale assessment of groundwater depletion and related groundwater abstractions: Combining hydrological modeling with information from well observations and GRACE satellites, Water Resources Research, 50, 5698–5720, https://doi.org/10.1002/2014WR015595, 2014.

Döll, P., Trautmann, T., Gerten, D., Schmied, H. M., Ostberg, S., Saaed, F., and Schleussner, C.-F.: Risks for the global freshwater system at 1.5 °C and 2 °C global warming, Environmental Research Letters, 13, 044038, https://doi.org/10.1088/1748-9326/aab792, 2018.

Douglas, E. M., Beltrán-Przekurat, A., Niyogi, D., Pielke, R. A., and Vörösmarty, C. J.: The impact of agricultural intensification and irrigation on land–atmosphere interactions and Indian monsoon precipitation — A mesoscale modeling perspective, Global and Planetary Change, 67, 117–128, https://doi.org/10.1016/j.gloplacha.2008.12.007, 2009.

Drewniak, B., Song, J., Prell, J., Kotamarthi, V. R., and Jacob, R.: Modeling agriculture in the Community Land Model, Geoscientific Model Development, 6, 495–515, https://doi.org/10.5194/gmd-6-495-2013, 2013.

Druel, A., Munier, S., Mucia, A., Albergel, C., and Calvet, J.-C.: Implementation of a new crop phenology and irrigation scheme in the ISBA land surface model using SURFEX_v8.1, Geoscientific Model Development, 15, 8453–8471, https://doi.org/10.5194/gmd-15-8453-2022, 2022.

Farquhar, G. D., von Caemmerer, S., and Berry, J. A.: A biochemical model of photosynthetic CO2 assimilation in leaves of C3 species, Planta, 149, 78–90, https://doi.org/10.1007/BF00386231, 1980.

Friedl, M., Sulla-Menashe, D.: MODIS/Terra+Aqua Land Cover Type Yearly L3 Global 500m SIN Grid V061. NASA EOSDIS Land Processes Distributed Active Archive Center [data set], https://doi.org/10.5067/MODIS/MCD12Q1.061, 2022

Gosling, S., Müller Schmied, H., Betts, R., Chang, J., Ciais, P., Dankers, R., Döll, P., Eisner, S., Flörke, M., Gerten, D., Grillakis, M., Hanasaki, N., Hagemann, S., Huang, M., Huang, Z., Jerez, S., Kim, H., Koutroulis, A., Leng, G., Liu, X., Masaki, Y., Montavez, P., Morfopoulos, C., Oki, T., Papadimitriou, L., Pokhrel, Y., Portmann, F. T., Orth, R., Ostberg, S., Satoh, Y., Seneviratne, S., Sommer, P., Stacke, T., Tang, Q., Tsanis, I., Wada, Y., Zhou, T., Büchner, M., Schewe, J., and Zhao, F.: ISIMIP2a Simulation Data from Water (global) Sector (V. 1.1), in, GFZ Data Services, https://doi.org/10.5880/PIK.2019.003, 2019.

GRDC: The Global Runoff Database, Global Runoff Data Centre [data set], https://www.bafg.de/GRDC/EN/Home/, 2023

Hanasaki, N., Yoshikawa, S., Pokhrel, Y., and Kanae, S.: A global hydrological simulation to specify the sources of water used by humans, Hydrology and Earth System Sciences, 22, 789–817, https://doi.org/10.5194/hess-22-789-2018, 2018.

Hanazaki, R., Yamazaki, D., and Yoshimura, K.: Development of a Reservoir Flood Control Scheme for Global Flood Models, Journal of Advances in Modeling Earth Systems, 14, e2021MS002944, https://doi.org/10.1029/2021MS002944, 2022.

https://doi.org/10.5194/egusphere-2024-4093
Preprint. Discussion started: 22 January 2025

Jägermeyr, J., Gerten, D., Heinke, J., Schaphoff, S., Kummu, M., and Lucht, W.: Water savings potentials of irrigation systems: global simulation of processes and linkages, Hydrology and Earth System Sciences, 19, 3073–3091, https://doi.org/10.5194/hess-19-3073-2015, 2015.

Jägermeyr, J., Müller, C., Ruane, A. C., Elliott, J., Balkovic, J., Castillo, O., Faye, B., Foster, I., Folberth, C., and Franke, J. A.: Climate impacts on global agriculture emerge earlier in new generation of climate and crop models, Nature Food, 2, 873–885, https://doi.org/10.1038/s43016-021-00400-y, 2021.

Jasechko, S., Seybold, H., Perrone, D., Fan, Y., Shamsudduha, M., Taylor, R. G., Fallatah, O., and Kirchner, J. W.: Rapid groundwater decline and some cases of recovery in aquifers globally, Nature, 625, 715–721, https://doi.org/10.1038/s41586-023-06879-8, 2024.

Jung, M., Koirala, S., Weber, U., Ichii, K., Gans, F., Camps-Valls, G., Papale, D., Schwalm, C., Tramontana, G., and Reichstein, M.: The FLUXCOM ensemble of global land-atmosphere energy fluxes, Scientific Data, 6, 74, https://doi.org/10.1038/s41597-019-0076-8, 2019.

Kang, S. and Eltahir, E. A. B.: North China Plain threatened by deadly heatwaves due to climate change and irrigation, Nature Communications, 9, 2894, https://doi.org/10.1038/s41467-018-05252-y, 2018.

Ketchum, D., Hoylman, Z. H., Huntington, J., Brinkerhoff, D., and Jencso, K. G.: Irrigation intensification impacts sustainability of streamflow in the Western United States, Communications Earth & Environment, 4, 1–8, https://doi.org/10.1038/s43247-023-01152-2, 2023.

Lehner, B., Liermann, C. R., Revenga, C., Vörösmarty, C., Fekete, B., Crouzet, P., Döll, P., Endejan, M., Frenken, K., Magome, J., Nilsson, C., Robertson, J. C., Rödel, R., Sindorf, N., and Wisser, D.: High-resolution mapping of the world's reservoirs and dams for sustainable river-flow management, Frontiers in Ecology and the Environment, 9, 494–502, https://doi.org/10.1890/100125, 2011.

Leng, G., Huang, M., Tang, Q., and Leung, L. R.: A modeling study of irrigation effects on global surface water and groundwater resources under a changing climate, Journal of Advances in Modeling Earth Systems, 7, 1285–1304, https://doi.org/10.1002/2015MS000437, 2015.

Leng, G., Leung, L. R., and Huang, M.: Significant impacts of irrigation water sources and methods on modeling irrigation effects in the ACME Land Model, Journal of Advances in Modeling Earth Systems, 9, 1665–1683, https://doi.org/10.1002/2016MS000885, 2017.

Li, C., Lu, H., Yang, K., Wright, J. S., Yu, L., Chen, Y., Huang, X., and Xu, S.: Evaluation of the Common Land Model (CoLM) from the Perspective of Water and Energy Budget Simulation: Towards Inclusion in CMIP6, Atmosphere, 8, 141, https://doi.org/10.3390/atmos8080141, 2017.

Li, C., Yuan, X., Jiao, Y., Ji, P., and Huang, Z.: High-resolution land surface modeling of the irrigation effects on evapotranspiration over the Yellow River basin, Journal of Hydrology, 633, 130986, https://doi.org/10.1016/j.jhydrol.2024.130986, 2024.

https://doi.org/10.5194/egusphere-2024-4093
Preprint. Discussion started: 22 January 2025

Li, D., Wrzesien, M. L., Durand, M., Adam, J., and Lettenmaier, D. P.: How much runoff originates as snow in the western United States, and how will that change in the future?, Geophysical Research Letters, 44, 6163–6172, https://doi.org/10.1002/2017GL073551, 2017.

Li, F., Zhou, Z., Levis, S., Sitch, S., Hayes, F., Feng, Z., Reich, P. B., Zhao, Z., and Zhou, Y.: Quantifying the role of ozone-caused damage to vegetation in the Earth system: a new parameterization scheme for photosynthetic and stomatal responses, Geoscientific Model Development, 17, 6173–6193, https://doi.org/10.5194/gmd-17-6173-2024, 2024.

Li, H., Huang, M., Wigmosta, M. S., Ke, Y., Coleman, A. M., Leung, L. R., Wang, A., and Ricciuto, D. M.: Evaluating runoff simulations from the Community Land Model 4.0 using observations from flux towers and a mountainous watershed, Journal of Geophysical Research: Atmospheres, 116, https://doi.org/10.1029/2011JD016276, 2011.

Li, H., Lo, M.-H., Ryu, D., Peel, M., and Zhang, Y.: Possible Increase of Air Temperature by Irrigation, Geophysical Research Letters, 49, e2022GL100427, https://doi.org/10.1029/2022GL100427, 2022.

Liang, X., Lettenmaier, D. P., Wood, E. F., and Burges, S. J.: A simple hydrologically based model of land surface water and energy fluxes for general circulation models, Journal of Geophysical Research: Atmospheres, 99, 14415–14428, https://doi.org/10.1029/94JD00483, 1994.

Lombardozzi, D. L., Lu, Y., Lawrence, P. J., Lawrence, D. M., Swenson, S., Oleson, K. W., Wieder, W. R., and Ainsworth, E. A.: Simulating Agriculture in the Community Land Model Version 5, Journal of Geophysical Research: Biogeosciences, 125, e2019JG005529, https://doi.org/10.1029/2019JG005529, 2020.

Lu, Y., Jin, J., and Kueppers, L. M.: Crop growth and irrigation interact to influence surface fluxes in a regional climate-cropland model (WRF3.3-CLM4crop), Climate Dynamics, 45, 3347–3363, https://doi.org/10.1007/s00382-015-2543-z, 2015.

Malek, K., Stöckle, C., Chinnayakanahalli, K., Nelson, R., Liu, M., Rajagopalan, K., Barik, M., and Adam, J. C.: VIC–CropSyst-v2: A regional-scale modeling platform to simulate the nexus of climate, hydrology, cropping systems, and human decisions, Geoscientific Model Development, 10, 3059–3084, https://doi.org/10.5194/gmd-10-3059-2017, 2017.

McDermid, S., Nocco, M., Lawston-Parker, P., Keune, J., Pokhrel, Y., Jain, M., Jägermeyr, J., Brocca, L., Massari, C., Jones, A. D., Vahmani, P., Thiery, W., Yao, Y., Bell, A., Chen, L., Dorigo, W., Hanasaki, N., Jasechko, S., Lo, M.-H., Mahmood, R., Mishra, V., Mueller, N. D., Niyogi, D., Rabin, S. S., Sloat, L., Wada, Y., Zappa, L., Chen, F., Cook, B. I., Kim, H., Lombardozzi, D., Polcher, J., Ryu, D., Santanello, J., Satoh, Y., Seneviratne, S., Singh, D., and Yokohata, T.: Irrigation in the Earth system, Nature Reviews Earth & Environment, 1–19, https://doi.org/10.1038/s43017-023-00438-5, 2023.

McDermid, S. S., Mearns, L. O., and Ruane, A. C.: Representing agriculture in Earth System Models: Approaches and priorities for development, Journal of Advances in Modeling Earth Systems, 9, 2230–2265, https://doi.org/10.1002/2016MS000749, 2017.

Mehta, P., Siebert, S., Kummu, M., Deng, Q., Ali, T., Marston, L., Xie, W., and Davis, K. F.: Half of twenty-first century global irrigation expansion has been in water-stressed regions, Nature Water, 2, 254–261, https://doi.org/10.1038/s44221-024-00206-9, 2024.

Merriam, J. L., Burt, C. M., Clemmens, A. J., Solomon, K. H., Howell, T. A., and Strelkoff, T. S.: Irrigation Performance Measures: Efficiency and Uniformity, Journal of Irrigation and Drainage Engineering, 125, 97–99, https://doi.org/10.1061/(ASCE)0733-9437(1999)125:2(97), 1999.

Mieno, T., Foster, T., Kakimoto, S., and Brozović, N.: Aquifer depletion exacerbates agricultural drought losses in the US High Plains, Nature Water, 2, 41–51, https://doi.org/10.1038/s44221-023-00173-7, 2024.

Müller Schmied, H., Cáceres, D., Eisner, S., Flörke, M., Herbert, C., Niemann, C., Peiris, T. A., Popat, E., Portmann, F. T., Reinecke, R., Schumacher, M., Shadkam, S., Telteu, C.-E., Trautmann, T., and Döll, P.: The global water resources and use model WaterGAP v2.2d: model description and evaluation, Geoscientific Model Development, 14, 1037–1079, https://doi.org/10.5194/gmd-14-1037-2021, 2021.

Muñoz-Sabater, J., Dutra, E., Agustí-Panareda, A., Albergel, C., Arduini, G., Balsamo, G., Boussetta, S., Choulga, M., Harrigan, S., Hersbach, H., Martens, B., Miralles, D. G., Piles, M., Rodríguez-Fernández, N. J., Zsoter, E., Buontempo, C., and Thépaut, J.-N.: ERA5-Land: a state-of-the-art global reanalysis dataset for land applications, Earth System Science Data, 13, 4349–4383, https://doi.org/10.5194/essd-13-4349-2021, 2021.

Nair, S., Johnson, J., and Wang, C.: Efficiency of Irrigation Water Use: A Review from the Perspectives of Multiple Disciplines, Agronomy Journal, 105, 351–363, https://doi.org/10.2134/agronj2012.0421, 2013.

Niu, G.-Y., Yang, Z.-L., Dickinson, R. E., and Gulden, L. E.: A simple TOPMODEL-based runoff parameterization (SIMTOP) for use in global climate models, Journal of Geophysical Research: Atmospheres, 110, https://doi.org/10.1029/2005JD006111, 2005.

Nocco, M. A., Smail, R. A., and Kucharik, C. J.: Observation of irrigation-induced climate change in the Midwest United States, Global Change Biology, 25, 3472–3484, https://doi.org/10.1111/gcb.14725, 2019.

Ozdogan, M., Rodell, M., Beaudoing, H. K., and Toll, D. L.: Simulating the Effects of Irrigation over the United States in a Land Surface Model Based on Satellite-Derived Agricultural Data, Journal of Hydrometeorology, 11, 171–184, https://doi.org/10.1175/2009JHM1116.1, 2010.

Pekel, J.-F., Cottam, A., Gorelick, N., and Belward, A. S.: High-resolution mapping of global surface water and its long-term changes, Nature, 540, 418–422, https://doi.org/10.1038/nature20584, 2016.

Phillips, C. E., Nair, U. S., Mahmood, R., Rappin, E., and Pielke, R. A.: Influence of Irrigation on Diurnal Mesoscale Circulations: Results From GRAINEX, Geophysical Research Letters, 49, e2021GL096822, https://doi.org/10.1029/2021GL096822, 2022.

https://doi.org/10.5194/egusphere-2024-4093
Preprint. Discussion started: 22 January 2025

Pokhrel, Y., Hanasaki, N., Koirala, S., Cho, J., Yeh, P. J.-F., Kim, H., Kanae, S., and Oki, T.: Incorporating Anthropogenic Water Regulation Modules into a Land Surface Model, Journal of Hydrometeorology, 13, 255–269, https://doi.org/10.1175/JHM-D-11-013.1, 2012.

Pokhrel, Y. N., Hanasaki, N., Wada, Y., and Kim, H.: Recent progresses in incorporating human land–water management into global land surface models toward their integration into Earth system models, WIREs Water, 3, 548–574, https://doi.org/10.1002/wat2.1150, 2016.

Puma, M. J. and Cook, B. I.: Effects of irrigation on global climate during the 20th century, Journal of Geophysical Research: Atmospheres, 115, https://doi.org/10.1029/2010JD014122, 2010.

Rappin, E. D., Mahmood, R., Nair, U. S., and Sr, R. A. P.: Land–Atmosphere Interactions during GRAINEX: Planetary Boundary Layer Evolution in the Presence of Irrigation, Journal of Hydrometeorology, 23, 1401–1417, https://doi.org/10.1175/JHM-D-21-0160.1, 2022.

Ruess, P. J., Konar, M., Wanders, N., and Bierkens, M. F. P.: Total irrigation by crop in the Continental United States from 2008 to 2020, Scientific Data, 11, 395, https://doi.org/10.1038/s41597-024-03244-w, 2024.

Russo, T. A. and Lall, U.: Depletion and response of deep groundwater to climate-induced pumping variability, Nature Geoscience, 10, 105–108, https://doi.org/10.1038/ngeo2883, 2017.

Sacks, W. J., Cook, B. I., Buenning, N., Levis, S., and Helkowski, J. H.: Effects of global irrigation on the near-surface climate, Climate Dynamics, 33, 159–175, https://doi.org/10.1007/s00382-008-0445-z, 2009.

Sacks, W. J., Deryng, D., Foley, J. A., and Ramankutty, N.: Crop planting dates: an analysis of global patterns, Global Ecology and Biogeography, 19, 607–620, https://doi.org/10.1111/j.1466-8238.2010.00551.x, 2010.

Schewe, J., Heinke, J., Gerten, D., Haddeland, I., Arnell, N. W., Clark, D. B., Dankers, R., Eisner, S., Fekete, B. M., Colón-González, F. J., Gosling, S. N., Kim, H., Liu, X., Masaki, Y., Portmann, F. T., Satoh, Y., Stacke, T., Tang, Q., Wada, Y., Wisser, D., Albrecht, T., Frieler, K., Piontek, F., Warszawski, L., and Kabat, P.: Multimodel assessment of water scarcity under climate change, Proceedings of the National Academy of Sciences, 111, 3245–3250, https://doi.org/10.1073/pnas.1222460110, 2014.

Schlosser, C. A., Strzepek, K., Gao, X., Fant, C., Blanc, É., Paltsev, S., Jacoby, H., Reilly, J., and Gueneau, A.: The future of global water stress: An integrated assessment, Earth's Future, 2, 341–361, https://doi.org/10.1002/2014EF000238, 2014.

Shangguan, W., Dai, Y., Duan, Q., Liu, B., and Yuan, H.: A global soil data set for earth system modeling, Journal of Advances in Modeling Earth Systems, 6, 249–263, https://doi.org/10.1002/2013MS000293, 2014.

Shen, X., Chen, Q., Sun, J., Huang, W., Gong, J., Li, Z., and Wang, J.: Development of Operational Global Medium-Range Forecast System in National Meteorological Centre, Meteorological Monthly, 47, 645–654, https://doi.org/10.7519/j.issn.1000-0526.2021.06.001, 2021.

https://doi.org/10.5194/egusphere-2024-4093
Preprint. Discussion started: 22 January 2025

Siebert, S. and Döll, P.: Quantifying blue and green virtual water contents in global crop production as well as potential production losses without irrigation, Journal of Hydrology, 384, 198–217, https://doi.org/10.1016/j.jhydrol.2009.07.031, 2010.

Siebert, S., Burke, J., Faures, J. M., Frenken, K., Hoogeveen, J., Döll, P., and Portmann, F. T.: Groundwater use for irrigation – a global inventory, Hydrology and Earth System Sciences, 14, 1863–1880, https://doi.org/10.5194/hess-14-1863-2010, 2010.

Siebert, S., Henrich, V., Frenken, K., and Burke, J.: Update of The Digital Global Map Of Irrigation Areas to Version 5, Rheinische Friedrich-Wilhelms-University, Bonn, Germany/Food and Agriculture Organization of the United Nations, Rome, Italy, 2013.

Sood, A. and Smakhtin, V.: Global hydrological models: a review, Hydrological Sciences Journal, 60, 549–565, https://doi.org/10.1080/02626667.2014.950580, 2015.

Sutanudjaja, E. H., van Beek, R., Wanders, N., Wada, Y., Bosmans, J. H. C., Drost, N., van der Ent, R. J., de Graaf, I. E. M., Hoch, J. M., de Jong, K., Karssenberg, D., López López, P., Peßenteiner, S., Schmitz, O., Straatsma, M. W., Vannametee, E., Wisser, D., and Bierkens, M. F. P.: PCR-GLOBWB 2: a 5 arcmin global hydrological and water resources model, Geoscientific Model Development, 11, 2429–2453, https://doi.org/10.5194/gmd-11-2429-2018, 2018.

Tang, Q., Oki, T., Kanae, S., and Hu, H.: The Influence of Precipitation Variability and Partial Irrigation within Grid Cells on a Hydrological Simulation, Journal of Hydrometeorology, 8, 499–512, https://doi.org/10.1175/JHM589.1, 2007.

Taranu, S. I., Lawrence, D. M., Wada, Y., Tang, T., Kluzek, E., Rabin, S., Yao, Y., De Hertog, S. J., Vanderkelen, I., and Thiery, W.: Bridging the gap: a new module for human water use in the Community Earth System Model version 2.2.1, Geoscientific Model Development, 17, 7365–7399, https://doi.org/10.5194/gmd-17-7365-2024, 2024.

Thiery, W., Davin, E. L., Lawrence, D. M., Hirsch, A. L., Hauser, M., and Seneviratne, S. I.: Present-day irrigation mitigates heat extremes, Journal of Geophysical Research: Atmospheres, 122, 1403–1422, https://doi.org/10.1002/2016JD025740, 2017.

USDA: National Agricultural Statistics Service Cropland Data Layer, Published crop-specific data layer, Washington, DC [data set], https://nassgeodata.gmu.edu/CropScape USDA-NASS, 2019.

USDA/NASS: Census of Agriculture, USDA - National Agricultural Statistics Service [data set], https://quickstats.nass.usda.gov/, 2023.

USGS: Water Use in the United States, USGS Water Data for the Nation [data set], https://water.usgs.gov/watuse/data/, 2023

Verma, S., Kumar, N., Verma, A., Singh, H., Siddique, K. H. M., and Singh, N. P.: Novel approaches to mitigate heat stress impacts on crop growth and development, Plant Physiology Reports, 25, 627–644, https://doi.org/10.1007/s40502-020-00550-4, 2020.

Vliet, M. T. H. van, Jones, E. R., Flörke, M., Franssen, W. H. P., Hanasaki, N., Wada, Y., and Yearsley, J. R.: Global water scarcity including surface water quality and expansions of

https://doi.org/10.5194/egusphere-2024-4093
Preprint. Discussion started: 22 January 2025

clean water technologies, Environmental Research Letters, 16, 024020, https://doi.org/10.1088/1748-9326/abbfc3, 2021.

de Vrese, P., Hagemann, S., and Claussen, M.: Asian irrigation, African rain: Remote impacts of irrigation, Geophysical Research Letters, 43, 3737–3745, https://doi.org/10.1002/2016GL068146, 2016.

de Vrese, P., Stacke, T., and Hagemann, S.: Exploring the biogeophysical limits of global food production under different climate change scenarios, Earth System Dynamics, 9, 393–412, https://doi.org/10.5194/esd-9-393-2018, 2018.

Weedon, G. P., Balsamo, G., Bellouin, N., Gomes, S., Best, M. J., and Viterbo, P.: The WFDEI meteorological forcing data set: WATCH Forcing Data methodology applied to ERA-Interim reanalysis data, Water Resources Research, 50, 7505–7514, https://doi.org/10.1002/2014WR015638, 2014.

Wisser, D., Fekete, B. M., Vörösmarty, C. J., and Schumann, A. H.: Reconstructing 20th century global hydrography: a contribution to the Global Terrestrial Network- Hydrology (GTN-H), Hydrology and Earth System Sciences, 14, 1–24, https://doi.org/10.5194/hess-14-1-2010, 2010.

Yamazaki, D., Kanae, S., Kim, H., and Oki, T.: A physically based description of floodplain inundation dynamics in a global river routing model, Water Resources Research, 47, https://doi.org/10.1029/2010WR009726, 2011.

Yamazaki, D., Ikeshima, D., Sosa, J., Bates, P. D., Allen, G. H., and Pavelsky, T. M.: MERIT Hydro: A High-Resolution Global Hydrography Map Based on Latest Topography Dataset, Water Resources Research, 55, 5053–5073, https://doi.org/10.1029/2019WR024873, 2019.

Yang, Y., Jin, Z., Mueller, N. D., Driscoll, A. W., Hernandez, R. R., Grodsky, S. M., Sloat, L. L., Chester, M. V., Zhu, Y.-G., and Lobell, D. B.: Sustainable irrigation and climate feedbacks, Nature Food, 4, 654–663, https://doi.org/10.1038/s43016-023-00821-x, 2023.

Yao, Y., Vanderkelen, I., Lombardozzi, D., Swenson, S., Lawrence, D., Jägermeyr, J., Grant, L., and Thiery, W.: Implementation and Evaluation of Irrigation Techniques in the Community Land Model, Journal of Advances in Modeling Earth Systems, 14, e2022MS003074, https://doi.org/10.1029/2022MS003074, 2022.

Yigzaw, W., Li, H.-Y., Demissie, Y., Hejazi, M. I., Leung, L. R., Voisin, N., and Payn, R.: A New Global Storage-Area-Depth Data Set for Modeling Reservoirs in Land Surface and Earth System Models, Water Resources Research, 54, 10,372-10,386, https://doi.org/10.1029/2017WR022040, 2018.

Yuan, X. and Liang, X.-Z.: Evaluation of a Conjunctive Surface–Subsurface Process Model (CSSP) over the Contiguous United States at Regional–Local Scales, Journal of Hydrometeorology, 12, 579–599, https://doi.org/10.1175/2010JHM1302.1, 2011.

Zhang, H., Zhang, M., Jin, J., Fei, K., Ji, D., Wu, C., Zhu, J., He, J., Chai, Z., Xie, J., Dong, X., Zhang, D., Bi, X., Cao, H., Chen, H., Chen, K., Chen, X., Gao, X., Hao, H., Jiang, J., Kong, X., Li, S., Li, Y., Lin, P., Lin, Z., Liu, H., Liu, X., Shi, Y., Song, M., Wang, H., Wang, T., Wang, X., Wang, Z., Wei, Y., Wu, B., Xie, Z., Xu, Y., Yu, Y., Yuan, L., Zeng, Q., Zeng, X.,

https://doi.org/10.5194/egusphere-2024-4093
Preprint. Discussion started: 22 January 2025

Zhao, S., Zhou, G., and Zhu, J.: Description and Climate Simulation Performance of CAS-ESM Version 2, Journal of Advances in Modeling Earth Systems, 12, e2020MS002210, https://doi.org/10.1029/2020MS002210, 2020a.

Zhang, Z., Barlage, M., Chen, F., Li, Y., Helgason, W., Xu, X., Liu, X., and Li, Z.: Joint Modeling of Crop and Irrigation in the central United States Using the Noah-MP Land Surface Model, Journal of Advances in Modeling Earth Systems, 12, e2020MS002159, https://doi.org/10.1029/2020MS002159, 2020b.

Zhao, G. and Gao, H.: Automatic Correction of Contaminated Images for Assessment of Reservoir Surface Area Dynamics, Geophysical Research Letters, 45, 6092–6099, https://doi.org/10.1029/2018GL078343, 2018.

Zhou, T., Leung, L. R., Leng, G., Voisin, N., Li, H.-Y., Craig, A. P., Tesfa, T., and Mao, Y.: Global Irrigation Characteristics and Effects Simulated by Fully Coupled Land Surface, River, and Water Management Models in E3SM, Journal of Advances in Modeling Earth Systems, 12, e2020MS002069, https://doi.org/10.1029/2020MS002069, 2020.